ACR No. L5F07a

NATIONAL ADVISORY COMMITTEE FOR AERONAUTICS

WARTIME REPORT

ORIGINALLY ISSUED
July 1945 as
Advance Confidential Report L5F07a

BLADE DESIGN DATA FOR AXIAL-FLOW FANS AND COMPRESSORS

By Seymour M. Bogdonoff and Harriet E. Bogdonoff

Langley Memorial Aeronautical Laboratory
Langley Field, Va.

NACA

WASHINGTON

NATIONAL ADVISORY COMMITTEE FOR AERONAUTICS

ADVANCE CONFIDENTIAL REPORT

BLADE DESIGN DATA FOR AXIAL-FLOW FANS AND COMPRESSORS

By Seymour M. Bogdonoff and Harriet E. Bogdonoff

SUMMARY

An experimental investigation to obtain blade design data for high-efficiency axial-flow fans and compressors was carried out in a two-dimensional low-speed cascade tunnel at the Langley laboratory of the NACA. The effects of camber, solidity, and stagger on blade turning angle and the shape of pressure distributions were determined for a family of five low-drag airfoils. These airfoils were cambered for free-air lift coefficients from 0 to 1.8 and were investigated at staggers of 45° and 60° and solidities of 1.0 and 1.5. Blade design charts for axial-flow fans and compressors were prepared that give the camber and angle-of-attack setting for any desired turning angle. Blades chosen from these design charts operate with an essentially flat pressure distribution. A test in a single-stage test blower showed that the maximum efficiency occurs near the point at which the pressure distribution is flat. Empirical equations are given by which the performance of an airfoil in cascade similar to those investigated may be predicted with sufficient accuracy for blade design.

INTRODUCTION

The increased demand for high-pressure and high-efficiency axial-flow compressors and fans, especially for gas-turbine and jet-propulsion engines, has necessitated an investigation of design problems. The present report provides aerodynamic information on airfoils suitable for use as blower blades. When the dimensions, speed, pressure rise, and mass flow of the compressor or fan are specified, these aerodynamic data can be used to design efficient blading.

[redacted]

The difficulties encountered in examining the flow around the rotating blades of a blower and in isolating three-dimensional effects make it advisable to do most of the testing on a stationary two-dimensional cascade of airfoils. Although conditions for a stationary cascade cannot exactly simulate those for rotating blades, the turning angles and the shapes of pressure distributions can be obtained with sufficient accuracy for use in the design of fans and compressors. The effects of changes in camber, angle of attack, stagger, and solidity on these blade characteristics were investigated and validated in a test made in the rotating setup. The present investigation is an extension of the work started in reference 1, in which an airfoil was tested at only one condition of stagger and solidity. The tests were made in a low-speed two-dimensional cascade tunnel and a single-stage test blower at the Langley Memorial Aeronautical Laboratory.

SYMBOLS

c_l	lift coefficient of isolated airfoil
c_{l_o}	lift coefficient referred to mean air
D_t	rotor-blade tip diameter, feet
F	force on blades, pounds
n	rotor speed, revolutions per second
p_1	static pressure ahead of blades, pounds per square foot
p_2	static pressure 1/2 chord behind blades, pounds per square foot
Δp	pressure rise across cascade (p_2-p_1), pounds per square foot
q	local dynamic pressure, pounds per square foot
q_1	dynamic pressure of entering air, pounds per square foot

q_2	dynamic pressure of air 1/2 chord behind blades, pounds per square foot
q_o	dynamic pressure of mean air, pounds per square foot
$\frac{\Delta p}{q_o}$	pressure-rise coefficient
Q	volume rate of flow, cubic feet per second
Q/nD_t^3	quantity coefficient
σ	solidity (chord of blade divided by gap between blades measured parallel to cascade)
S	blade area, square feet
U	velocity of rotor blade element at radius r, feet per second
V_2	velocity of air behind blade relative to casing, feet per second
V_a	velocity in axial direction, feet per second
W_1	velocity of entering air relative to rotor, feet per second
W_2	velocity of air behind blades relative to rotor, feet per second
W_o	mean velocity, 1/2 of vector sum of W_1 and W_2, feet per second
ΔW	change in tangential velocity (velocity parallel to cascade), feet per second
x	chordwise distance from leading edge
y	vertical distance from chord
α	angle between entering air and chord line of blade
α_d	design angle of attack of airfoil in cascade (with respect to entering air)
α_o	angle between mean air and chord line of the blade

[redacted]

α_i design angle of attack of isolated airfoil

α_{l_0} angle of zero lift for isolated airfoil

β stagger angle, angle between perpendicular to cascade and entering air

β_0 mean stagger angle, angle between perpendicular to cascade and mean air

δ ratio of change in tangential component of velocity to axial velocity

η adiabatic efficiency of rotor (reference 3)

θ angle through which air is turned by blades, degrees

ρ mass density of air, slugs per cubic foot

DESCRIPTION OF TEST APPARATUS

Cascade tests.- A vertical cross section of the low-speed two-dimensional cascade tunnel used in the present investigation is shown in figure 1. The tunnel was so constructed that data could be obtained for any desired stagger or solidity, and the airfoils were mounted to allow changes in the angles of attack relative to the incoming air. From the region A, which was kept above atmospheric pressure by a 25-horsepower blower, the air passed through two 30-mesh screens into a large settling chamber. Since laminar-flow regions probably would not be encountered in an actual blower, a $\frac{1}{4}$-inch screen was inserted at the entrance to the test section to introduce a small amount of turbulence.

Boundary-layer suction slots, 3/16 inch wide, were built into the side walls 1 chord length ahead of and parallel to the cascade of airfoils. This arrangement may be seen in the horizontal cross section of the tunnel shown in figure 2. By varying the speed of a centrifugal blower attached to the suction chambers, flow through the slots was controlled. With the tunnel empty, the flow was adjusted to make the static pressures along the axis

[redacted]

of the tunnel approximately constant. When this condition was satisfied, a yaw survey downstream of the slot showed that the flow was parallel to the top and bottom floors. Flexible plates attached to the rigid floors extended from 1 chord length ahead of the blades to approximately 1/2 chord length downstream (fig. 1).

The blade sections tested were NACA 65(216)-series airfoils scaled down to 10-percent thickness and cambered for a uniform load along the chord ($a = 1.0$, reference 2). The trailing edges of these airfoils were thickened to make a more practical section by the addition of 0.0015x (where x is the percent-chord position) to the thickness-distribution ordinates. These altered airfoils are known as the NACA 65-series blower-blade sections (reference 1). The blade sections tested, of 5-inch chord and span, were cambered for free-air lift coefficients of 0, 0.4, 0.8, 1.2, and 1.8. Ordinates of the airfoils are presented in tables I to V; cross sections of the airfoils are shown in figure 3.

Blower tests.- The blades for the blower tests were designed from the two-dimensional blade-section data in order to set up vortex flow. A sample calculation to show how blade camber and angle-of-attack setting were determined is found in the appendix. Blades having a constant chord of 3 inches and a solidity of 1.0 at the pitch section (located halfway between the root and the tip) were used. The blades operated with a clearance of approximately 0.016 inch between the tips of the blades and the casing. These blower tests were made in the single-stage test blower shown schematically in figure 4. The tip diameter was 27.82 inches; the hub diameter, 21.82 inches. All tests were made at a rotational speed of 2405 rpm.

TESTING METHODS

Cascade tests.- After the tunnel walls of the low-speed two-dimensional cascade tunnel had been rotated to give the desired stagger, the cascade of five airfoils, spaced to give the correct solidity, was sealed to the walls without fillets. Each of the blades was tested at staggers of 45° and 60° and at solidities of 1.0 and 1.5. The flexible floors of the tunnel were adjusted to give the following conditions of an infinite cascade: (a) constant static pressure 1/2 chord length ahead of the blades, (b) constant angle of entering air along the cascade, and (c) constant angle (averaged behind each blade) of exit air along the cascade. Condition (b) was checked by measurements with yaw tubes 1/2 chord length ahead of the blades at four stations along the cascade. These yaw tubes were used only to set the flexible floors and were removed before measurements in the cascade were taken. Condition (c) was checked by a survey 1/2 chord length behind the blades.

Pressures ahead of the cascade were measured by two total-head tubes and the row of wall static-pressure orifices shown in figure 1. The static pressure 1/2 chord length behind the blades was assumed to be atmospheric (reference 1). Turning angles were measured by surveying the central vertical plane along the cascade with a cylindrical yaw tube. The yaw tube was 1/4 inch in diameter with two static-pressure orifices set at an included angle of 80°. The "null" method of taking measurements was used; that is, the tube was rotated until both static-pressure orifices registered equal pressures. Pressure distributions were obtained from the center airfoil, which was equipped with pressure orifices. These measurements were taken over a range of angle of attack α that includes conditions from a pressure distribution with a pronounced peak on the lower surface to a pressure distribution with either a pronounced peak on the upper surface or stalled flow. All tests were run at a Reynolds number of approximately 300,000 and a Mach number of approximately 0.1 based on mean-air conditions.

Blower tests.- In the single-stage test blower, radial surveys of total pressure, static pressure, and yaw angle were made 1 chord length upstream and downstream of the blades. The power input was calculated from the amount of rotation added to the air. Entrance conditions to the rotor were set by varying the axial velocity through the blower by throttling the inlet (changing the area of the entrance ports (fig. 4)). This test was run at a Reynolds number of approximately 500,000 and a Mach number of approximately 0.27, both based on mean-air conditions relative to the rotor.

PRESENTATION OF DATA AND DISCUSSION

Turning angles.- From stationary two-dimensional cascade tests, the angle through which the air was turned θ was found for a range of airfoil angle of attack α. These data are presented in figures 5 to 8. Repeat runs indicated that these results were consistent within $\pm\frac{1}{2}^{\circ}$. The cascade, within the scope and experimental accuracy of the investigation, shows the characteristics of the infinite-solidity case; that is, $d\theta/d\alpha$ is close to unity.

Although the tests of the symmetrical blades are of little general use in the design of blower blades, an examination of the tests shows the effect of blade thickness on turning angle. The plots of turning angle against angle of attack for these airfoils (figs. 5 to 8) ~~show~~ that, at $\alpha = 0^{\circ}$, there is a definite amount of turning of the air in a direction opposite to that induced by cambering the airfoils. This negative value of θ, which indicates a pressure drop, becomes more negative with increasing solidity and stagger. This effect may be expected upon consideration of the velocities induced by a cascade of blades of finite thickness set at a stagger. The effect will decrease with decreases in thickness.

The variation of turning angle along the blade from yaw surveys behind the rotor in the single-stage test blower are presented in figure 9. These results are for the rotor blades operating approximately 4.8° above and 2.7° and 5.2° below the design angle of attack (10.2°). The broken-line curves are for the angles predicted from the two-dimensional cascade studies. The test points presented are for regions in which the blade operated outside the wall boundary layer. The predicted angles for these points check the measured angles within approximately 1°. The effects of tip clearance may be the cause of the larger deviation at the tip.

Reference 1 presents a simple equation for the prediction of turning angles that, for the range tested, gave fairly accurate results. This equation is of the form

$$\theta = k(\alpha - \alpha_{l_o})$$

[redacted]

The values of the empirical factor k, including the one evaluated in reference 1, are presented in the following table:

Stagger (deg)	Solidity	k
45	1.0	0.9
45	1.5	1.0
60	1.0	.75
60	1.5	.9

An approximate zero-lift angle can be calculated by use of an actual lift coefficient equal to 60 percent of the theoretical lift coefficient at zero angle of attack and an average slope of 0.09 for the lift curve. These values were obtained from the tests presented herein for the family of isolated airfoils in the cascade tunnel.

By use of these empirical relations, the turning angle for cambered blades in the range tested may be predicted to within approximately 1°.

<u>Pressure distributions</u>.- The pressure distributions over the center blade of the cascades are presented in figures 10 to 29, in which the ratio of local dynamic pressure to mean dynamic pressure is plotted against percent-chord position. These pressure distributions cannot be used to get lift coefficients because of an erroneous pressure rise (discussed in the section entitled "Pressure rise"). The shape of the diagram, however, is essentially correct. By an arbitrary resetting of the ends of the flexible floors, the pressure rises could be changed ±15 percent without affecting the shape of the pressure distributions or the turning angle. This insensitivity may be due to the large boundary layers on the walls and floors. Since the shapes may be assumed correct, they are used to indicate good operating angles of attack. The angle of attack at which a flat pressure distribution (approximately uniform load with no peaks) was obtained was designated the design point. On each side of this design point, there is a range of approximately 3° in which no pronounced

peaks are encountered. This range varied with the camber of the blades and with the entrance conditions.

An examination of the distributions shows that the loadings of the high-cambered blades - the NACA 65-(12)10 and the NACA 65-(18)10 blades (figs. 22 to 29) - were not so uniform as the low-camber blades but dropped over the back half of the airfoil. The same effect occurs for the isolated airfoils (figs. 30 to 34).

The theory by which these airfoils were cambered is essentially a thin-airfoil theory and does not apply to high cambers. The airfoils are also designed on the assumption of constant velocity in the stream and flow parallel at some distance ahead of and behind the airfoil. The blade, in cascade, operates in a region in which the velocity is decreasing and the streamlines ahead of and behind the cascade are usually not parallel. These differences between cascade and isolated-airfoil conditions further unload the rear portion of the airfoil. In order to obtain uniform loading for high-cambered blades in cascade, a new method of cambering that presupposes cascade operating conditions must be developed.

For the 60°-stagger case, the flat pressure distribution could not be obtained at any angle of attack, although some distributions did not show sharp peaks. For the NACA 65-(18)10 blade, flow over the top surface stalled before the high peak on the bottom surface had disappeared (figs. 28 and 29). It has not been definitely ascertained that this stalling is due entirely to the blade. The stalling of the flow over the top surface might have been caused by the stalling of the walls and wall-blade junctures, which could not support the extremely high pressure rise. A single test was made with roughness strips on the leading edge of the blades to simulate Reynolds numbers higher than the usual operating value (fig. 29) but no noticeable effects were found. Further tests in a rotating machine seem necessary to validate these data.

Pressure rise.- The pressure rises measured in the low-speed two-dimensional cascade tunnel were found to be lower than those measured in the rotating setup. A rough evaluation of the pressure-rise coefficient from the low-speed two-dimensional cascade tests was made corresponding to the conditions at the root, pitch, and tip of the rotor blade at an angle of attack 2.7° below the design angle of attack. These values were $\Delta p/q_o = 0.326$, 0.314, and 0.290, respectively; whereas the test-blower pressure-rise coefficient at the pitch section was equal to 0.360 (fig. 35). This low pressure rise predicted from cascade tests may be attributed to one or both of the following causes: (a) The flexible floors can be adjusted to satisfy the conditions of an infinite cascade ahead of the blades and to give a constant but not correct static pressure behind the blades. This condition was shown by a changing of the setting of the flexible floors (mentioned in the section entitled "Pressure distribution"). (b) The boundary-layer slots remove the boundary layer on the walls developed up to the slot. In the distance from the slots to the blades, however, new boundary layers develop on the walls. In going through the cascade, the air passing over the blades starts with a zero-thickness boundary layer on the leading edge. The walls, which experience the same pressure rise as the blades, incur high losses due to the already well-developed boundary layer. In the extreme cases, the wall boundary layers actually separated while the blades were still unstalled. These losses resulted in a decrease in the pressure rise obtained. In comparison with the effects of the wall boundary layer, the effects of the blade boundary layer were small.

The ratio of the theoretical pressure rise to the mean dynamic pressure may be calculated from

$$\frac{\Delta p}{q_o} = \frac{W_1^2 - W_2^2}{W_o^2} \tag{1a}$$

or, in terms of the angles,

$$\frac{\Delta p}{q_o} = \cos^2\beta_o\left[\frac{1}{\cos^2\beta} - \frac{1}{\cos^2(\beta - \theta)}\right] \tag{1b}$$

(See fig. 15.) This equation, which is calculated from the simple Bernoulli equation (reference 1), assumes incompressible flow and no losses. Equations (1) can be used to calculate the pressure rise through a rotor, if velocities and angles are taken relative to the rotor. These theoretical pressure-rise coefficients (fig. 35) were calculated from the turning angles predicted on the basis of two-dimensional tests for the three conditions at which pressures were measured in the test blower. The test points show that approximately 90 percent of the theoretical pressure rise is obtained if the blade is operating at or near the maximum efficiency. It is thus evident that the theoretical pressure rise gives a more accurate approximation than the cascade tests to actual measurements. The plots show deviations caused by tip clearance similar to those of the turning-angle plots (fig. 9).

Lift coefficient.- If the drag forces are neglected, the lift of a blade in cascade may be resolved into two components: (1) the force parallel to the stagger line (line parallel to the row of blades) due to turning of the air and (2) the force perpendicular to the stagger line due to the pressure rise. Since the pressure rise measured in cascade is low, the lift coefficients calculated from these tests also will be low. This low pressure rise also invalidated the use of the pressure distribution for this calculation.

The theoretical lift coefficient of an airfoil in cascade based on mean velocity, with no losses and with incompressible flow assumed, may be calculated from the following equation (similar to equation (4) in reference 1):

$$c_{l_\sigma}{}^2 = \frac{F^2}{(q_o S)^2} = \left(\frac{2\delta V_a{}^2}{W_o{}^2\sigma}\right)^2 + \left(\frac{\Delta p}{q_o\sigma}\right)^2$$

which reduces to

$$c_{l_\sigma} = \frac{2\delta V_a}{W_o\sigma}$$

The lift coefficient for blade sections of the test blower may be calculated by use of the theoretical pressure rise and the predicted turning angles. These calculated coefficients will be accurate within 5 to 10 percent, since the actual pressure near design is 90 percent of the theoretical pressure and the actual turning angles check the predicted angles within 1°. A plot of c_{l_o} against θ is shown in figure 37 so that, if desired, the data may be interpreted in terms of c_{l_o}.

Lift coefficients for the isolated-airfoil tests were calculated from the pressure distributions and are plotted against angle of attack in figure 38. For the type of loading used ($a = 1.0$, reference 2), the angle of attack at which the theoretical pressure distribution and c_l should be obtained is zero. For low camber (low theoretical lift coefficients) this angle actually falls between 0° and 2°. The tests of the high-cambered airfoils, however, show that the deviation increases with camber; for the NACA 65-(18)10 blower blade, a pressure distribution similar in shape to the theoretical pressure distribution is not obtained until an angle of attack of $5\frac{1}{2}°$ is reached. Approximately 60 percent of the theoretical lift is obtained at $\alpha = 0°$. In figure 39, the c_{l_o} for the design points in cascade is plotted against the theoretical design c_l for the isolated airfoil. For all cases except that in which $\beta = 45°$ and $\sigma = 1.0$, the limiting cascade c_{l_o} is approached. When $\beta = 45°$ and $\sigma = 1.0$, the curve seems to indicate that some gain may be made by blades of higher camber than those tested herein. This curve shows also that, for high cambers, the design lift coefficient in cascade is considerably below that of the isolated airfoil. The basis for blade comparison is thus not directly lift coefficient but the pressure rise that the blade can withstand without stalling. For example, the NACA 65-(18)10 blades stalled in cascade at $\beta = 60°$, whereas the isolated airfoil was completely unstalled. This pressure rise is the sum of the pressure rise due to turning and that due to the load and thickness distributions of the blade. The results obtained indicate that thinner blades would be better for high-pressure-rise conditions, but the consequent smaller nose radius would decrease the range of peak-free operation.

<u>Design conditions and efficiency</u>.- From the data available on low-drag airfoils (reference 2), it is evident that minimum drag occurs when the airfoil pressure distribution is essentially flat - that is, when no

velocity peaks are experienced. Since achievement of high efficiency was one aim of the present investigation, this flat distribution was taken as the design point. The advantages of operating at this design point can be seen from a comparison of two designs having the same lift. The blade operating with a flat distribution will have lower losses and therefore higher efficiency than a blade with a peaked distribution. The blade with flat distribution will also allow higher rotational speeds before the critical speed is reached and consequently will give higher pressure rises per stage. This use of a flat pressure distribution to attain high efficiencies was shown in the blower tests. The efficiency measured at this design point is very close to the maximum efficiency (fig. 40). The design blade-operating angle of attack and the volume flow check those at maximum efficiency within the experimental accuracy ($\pm 0.5^\circ$ for turning angles, ± 0.7 percent for efficiencies).

The design point for each blade at each condition was obtained from an examination of the pressure distributions and is noted on each figure (figs. 10 to 29). These data are presented in the form of design charts (figs. 41(a) and 41(b)). The charts are derived for the family of airfoils within the range of entrance conditions tested. Little is known of the effects of changes in blade thickness and load distribution. If entrance conditions are known, the designer can select the camber and angle-of-attack setting for any desired turning angle from the charts. This process may be reversed if the best performance of a given blade is desired.

For the design points, the angle of attack of the isolated airfoil was found to be approximately 2° lower than the angle of attack with respect to the mean air of the airfoil in cascade. The design angle of attack in free air may be obtained from the equation

$$\alpha_i = 3c_l + 0.5^\circ$$

which is derived from the isolated-airfoil tests. By use of these relations to predict the angle of attack for the design pressure distribution in free air and in cascade and by use of the empirical equation for turning angle, the performance of an airfoil in cascade near maximum efficiency may be predicted with sufficient accuracy for low-drag airfoils of the type investigated.

[redacted]

In reference 1, approximate evaluations of the losses through a cascade were made from total-pressure surveys and pressure-rise measurements. These results agreed at the one angle investigated, but subsequent tests have not validated this agreement. The pressure-rise data usually showed considerably higher losses than the total-pressure surveys. Since the blade losses are dependent on the pressure rise experienced by the blade, no efficiency measurements can be obtained from the stationary-cascade data.

APPLICATION OF DATA

A sample calculation of the design for a typical blade section is shown in the appendix. This design corresponds approximately to the design of the pitch section of the blade tested in the single-stage test blower. In the design of a blower, certain specifications must be met - for example, the entrance conditions, the pressure rise, the rotational speed, and perhaps the number of blades. A vector diagram corresponding to the entrance conditions and similar to the diagram in figure 42 may be set up. Since the pressure rise and entrance velocity are known, the exit velocity may be calculated from

$$\Delta p = \frac{1}{2}\rho\left(W_1{}^2 - W_2{}^2\right)$$

assumes zero static pressure rise
Total pressure rise given by velocity change

by the use of an average value of density calculated from entrance and exit pressures. After the velocities are known, the turning angle and the stagger can be calculated from simple trigonometric relations. The chosen solidity can be checked only by a completion of the design to see if it will give the desired performance within the range covered by the charts.

The design camber (in terms of the theoretical c_l of the isolated airfoil) is found from the design chart (fig. 41(a)) by use of the entrance conditions and the calculated turning angle. On a vertical line drawn through the turning-angle value, an interpolation is made for stagger. From this point, a horizontal line is drawn until it intersects the set of curves on the right of the figure. Along this horizontal line, an interpolation is made for solidity and stagger. The resulting point gives the design camber of the blades. On the second design curve (fig. 41(b)), a vertical line is drawn through the camber just determined and an interpolation is made for stagger. At the located point, a horizontal line is drawn intersecting the curves on the right where a horizontal interpolation is then made for solidity. This final point gives the angle-of-attack setting for the blade.

The procedure may be repeated for as many blade sections as desired for the setting up of any required flow pattern. For most cases, however, it is sufficient to design the blade at three sections and fair among them.

CONCLUDING REMARKS

An experimental investigation of the characteristics of a family of low-drag airfoils in cascade and in free air was made in a two-dimensional low-speed cascade tunnel at the Langley laboratory of the NACA. Based upon this investigation, design charts are presented which, if the operating parameters are known, will give fan and compressor blades and settings for high-efficiency operation. The charts are derived from two-dimensional tests to give blades operating with an essentially flat pressure distribution.

Langley Memorial Aeronautical Laboratory
National Advisory Committee for Aeronautics
Langley Field, Va.

APPENDIX

SAMPLE BLADE-SECTION CALCULATION

Data given.- The following data are given for the sample blade-section calculation:

Mass density of air, ρ, slug/cu ft	0.002378
Pressure rise, Δp, lb/sq ft	50
Solidity, σ	1.0
Axial velocity, V_a, ft/sec	220
Rotational speed, U, ft/sec	260

Procedure.- From the equation

$$\Delta p = \frac{1}{2}\rho\left(W_1^2 - W_2^2\right)$$

the velocity leaving the rotor W_2 may be calculated to be equal to 272 feet per second. These data are now sufficient to draw the following vector diagram of the flow entering and leaving the rotor:

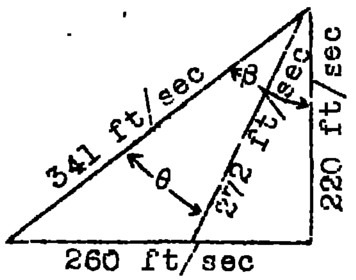

From this diagram, the angles β and θ may be calculated as $\beta = 49.75^\circ$ and $\theta = 13.75^\circ$.

In figure 41(a) a vertical line is drawn through $\theta = 13.75^\circ$ and an interpolation is made along this line for $\beta = 49.75^\circ$. Through this point a horizontal line is drawn to intersect the set of curves on the right. Since the solidity is equal to 1.0, no interpolation is necessary and a camber of 0.81 (design c_l in free air) is obtained.

[redacted]

On the second curve (fig. 41(b)), a vertical line is drawn through the camber just determined (0.81) and an interpolation is made for $\beta = 49.75^{\circ}$. A horizontal line is now drawn through the point just determined to intersect the set of curves on the right. A horizontal interpolation for solidity (no interpolation in this case) gives for the airfoil an angle of attack of 11.2° with respect to the incoming air.

REFERENCES

1. Kantrowitz, Arthur, and Daum, Fred L.: Preliminary Experimental Investigation of Airfoils in Cascade. NACA CB, July 1942.

2. Abbott, Ira H., von Doenhoff, Albert E., and Stivers, Louis S., Jr.: Summary of Airfoil Data. NACA ACR No. L5C05, 1945.

3. Sinnette, John T., Jr., Schey, Oscar W., and King, J. Austin: Performance of NACA Eight-Stage Axial-Flow Compressor Designed on the Basis of Airfoil Theory. NACA ACR No. E4H18, 1944.

TABLE I

ORDINATES FOR NACA 65-010 BLOWER BLADE

[Derived from NACA 65(216)-010 airfoil combined with y = 0.0015x; stations and ordinates in percent of chord]

Upper surface		Lower surface	
x	y	x	y
0	0	0	0
.5	.752	.5	-.752
.75	.890	.75	-.890
1.25	1.124	1.25	-1.124
2.5	1.571	2.5	-1.571
5.0	2.222	5.0	-2.222
7.5	2.709	7.5	-2.709
10	3.111	10	-3.111
15	3.746	15	-3.746
20	4.218	20	-4.218
25	4.570	25	-4.570
30	4.824	30	-4.824
35	4.982	35	-4.982
40	5.057	40	-5.057
45	5.029	45	-5.029
50	4.870	50	-4.870
55	4.570	55	-4.570
60	4.151	60	-4.151
65	3.627	65	-3.627
70	3.038	70	-3.038
75	2.451	75	-2.451
80	1.847	80	-1.847
85	1.251	85	-1.251
90	.749	90	-.749
95	.354	95	-.354
100	.150	100	-.150
L.E. radius: 0.666			

NATIONAL ADVISORY
COMMITTEE FOR AERONAUTICS

TABLE II

ORDINATES FOR NACA 65-410 BLOWER BLADE

[Derived from NACA 65(216)-410 airfoil combined with y = 0.0015x; stations and ordinates in percent of chord]

Upper surface		Lower surface	
x	y	x	y
0	0	0	0
.375	.842	.625	-.642
.613	1.020	.887	-.740
1.095	1.327	1.405	-.899
2.318	1.932	2.682	-1.188
4.793	2.844	5.207	-1.580
7.284	3.548	7.716	-1.852
9.783	4.137	10.217	-2.069
14.793	5.086	15.207	-2.394
19.814	5.806	20.186	-2.622
24.840	6.357	25.160	-2.777
29.870	6.765	30.130	-2.877
34.902	7.044	35.098	-2.924
39.935	7.199	40.065	-2.915
44.968	7.219	45.032	-2.839
50.000	7.076	50.000	-2.664
55.029	6.762	54.971	-2.382
60.054	6.291	59.946	-2.007
65.071	5.686	64.918	-1.566
70.082	4.994	69.918	-1.106
75.086	4.238	74.914	-.658
80.081	3.434	79.919	-.250
85.070	2.607	84.930	.085
90.052	1.781	89.948	.287
95.033	.985	94.967	.279
100.033	.146	99.967	-.146
L.E. radius: 0.666			

NATIONAL ADVISORY
COMMITTEE FOR AERONAUTICS

[redacted]

TABLE III

ORDINATES FOR NACA 65-810 BLOWER BLADE

[Derived from NACA 65(216)-810 airfoil combined with y = 0.0015x; stations and ordinates in percent of chord]

Upper surface		Lower surface	
x	y	x	y
0	0	0	0
.260	.913	.740	-.513
.486	1.130	1.014	-.570
.949	1.510	1.551	-.654
2.143	2.274	2.857	-.786
4.591	3.448	5.409	-.920
7.072	4.371	7.928	-.979
9.569	5.149	10.431	-1.013
14.589	6.415	15.411	-1.031
19.629	7.386	20.371	-1.018
24.681	8.139	25.319	-.979
29.740	8.705	30.260	-.929
34.804	9.098	35.196	-.858
39.870	9.339	40.130	-.771
44.936	9.409	45.064	-.649
50.000	9.282	50.000	-.458
55.058	8.950	54.942	-.190
60.107	8.434	59.893	.134
65.143	7.744	64.857	.496
70.164	6.922	69.836	.854
75.171	6.025	74.829	1.135
80.162	5.024	79.838	1.344
85.137	3.935	84.863	1.449
90.104	2.810	89.896	1.326
95.065	1.612	94.935	.916
100.048	.142	99.952	-.142
L.E. radius: 0.666			

NATIONAL ADVISORY
COMMITTEE FOR AERONAUTICS

TABLE IV

ORDINATES FOR NACA 65-(12)10 BLOWER BLADE

[Derived from NACA 65(216)-(12)10 airfoil combined with y = 0.0015x; stations and ordinates in percent of chord]

Upper surface		Lower surface	
x	y	x	y
0	0	0	0
.161	.971	.839	-.371
.374	1.227	1.126	-.387
.817	1.679	1.683	-.395
1.981	2.599	3.019	-.367
4.399	4.035	5.601	-.243
6.868	5.178	8.132	-.090
9.361	6.147	10.639	.057
14.388	7.734	15.612	.342
19.477	8.958	20.553	.594
24.523	9.915	25.477	.825
29.611	10.640	30.389	1.024
34.706	11.153	35.294	1.207
39.804	11.479	40.196	1.373
44.904	11.598	45.096	1.542
50.000	11.488	50.000	1.748
55.087	11.139	54.913	2.001
60.161	10.574	59.839	2.278
65.214	9.801	64.786	2.559
70.245	8.860	69.755	2.804
75.256	7.808	74.744	2.932
80.242	6.607	79.758	2.945
85.204	5.272	84.796	2.804
90.154	3.835	89.846	2.369
95.096	2.237	94.904	1.555
100.068	.134	99.932	-.134
L.E. radius: 0.666			

NATIONAL ADVISORY
COMMITTEE FOR AERONAUTICS

[redacted]

TABLE V

ORDINATES FOR NACA 65-(18)10 BLOWER BLADE

[Derived from NACA 65(216)-(18)10 airfoil combined with y = 0.0015x; stations and ordinates in percent of chord]

Upper surface		Lower surface	
x	y	x	y
0	0	0	0
.046	1.049	.954	-.149
.240	1.359	1.260	-.099
.654	1.916	1.846	.010
1.770	3.065	3.230	.283
4.137	4.891	5.863	.797
6.583	6.365	8.417	1.267
9.066	7.620	10.934	1.686
14.097	9.692	15.903	2.422
19.179	11.301	20.821	3.027
24.289	12.569	25.711	3.541
29.419	13.537	30.581	3.959
34.560	14.233	35.440	4.307
39.707	14.688	40.293	4.590
44.856	14.882	45.144	4.828
50.000	14.797	50.000	5.057
55.131	14.423	54.869	5.287
60.241	13.783	59.759	5.495
65.320	12.883	64.680	5.657
70.381	11.764	69.634	5.732
75.381	10.476	74.619	5.634
80.360	8.976	79.640	5.352
85.302	7.271	84.698	4.843
90.225	5.367	89.775	3.939
95.138	3.170	94.862	2.518
100.091	.120	99.909	-.120
L.E. radius: 0.666			

NATIONAL ADVISORY
COMMITTEE FOR AERONAUTICS

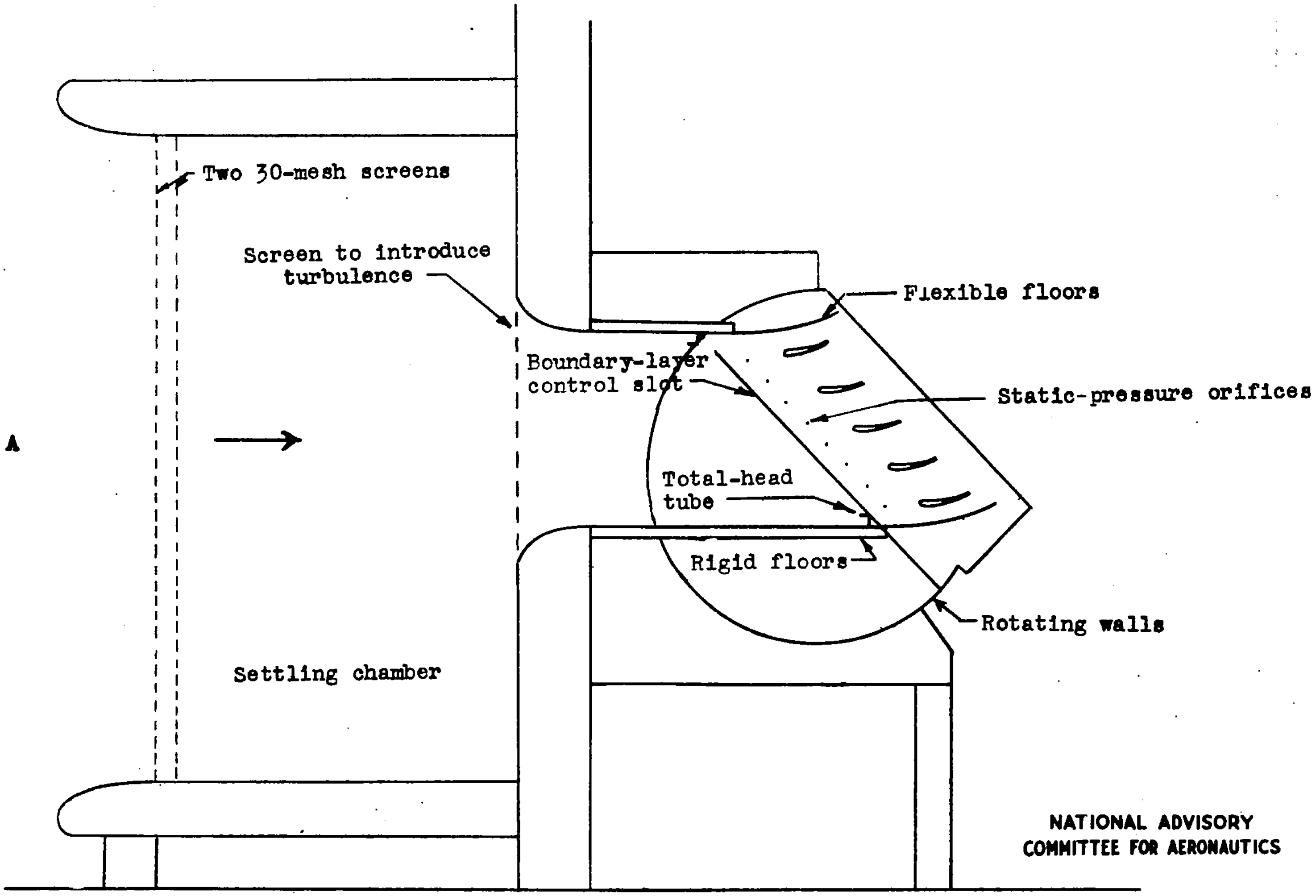

Figure 1.- Vertical cross section of two-dimensional low-speed cascade tunnel.

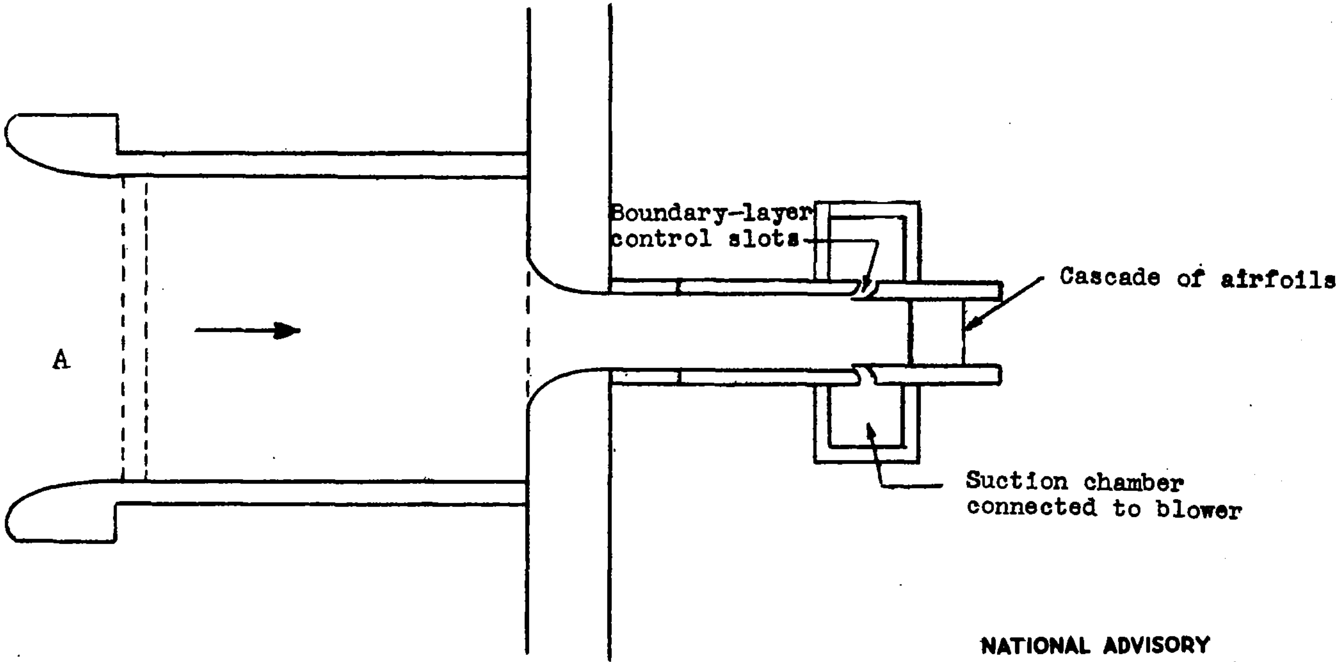

NATIONAL ADVISORY
COMMITTEE FOR AERONAUTICS

Figure 2.- Horizontal cross section of two-dimensional low-speed cascade tunnel.

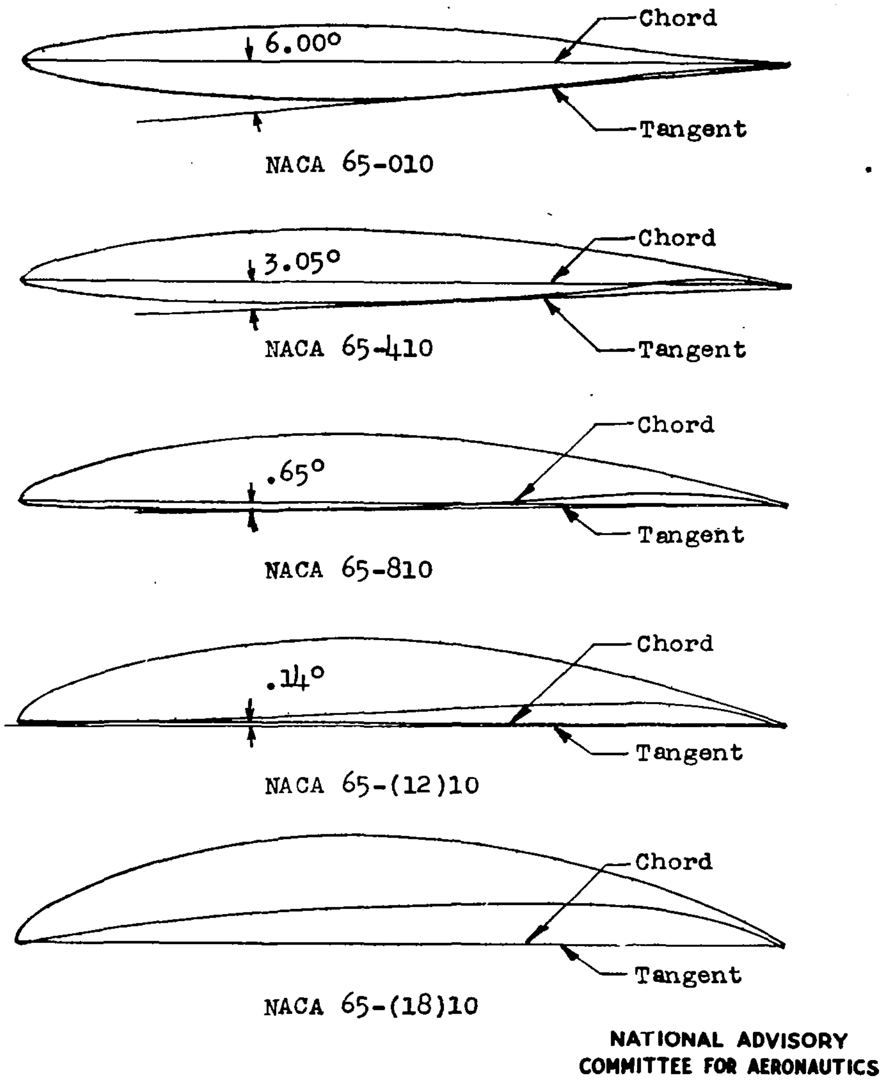

Figure 3.- NACA 65-series blower-blade sections.

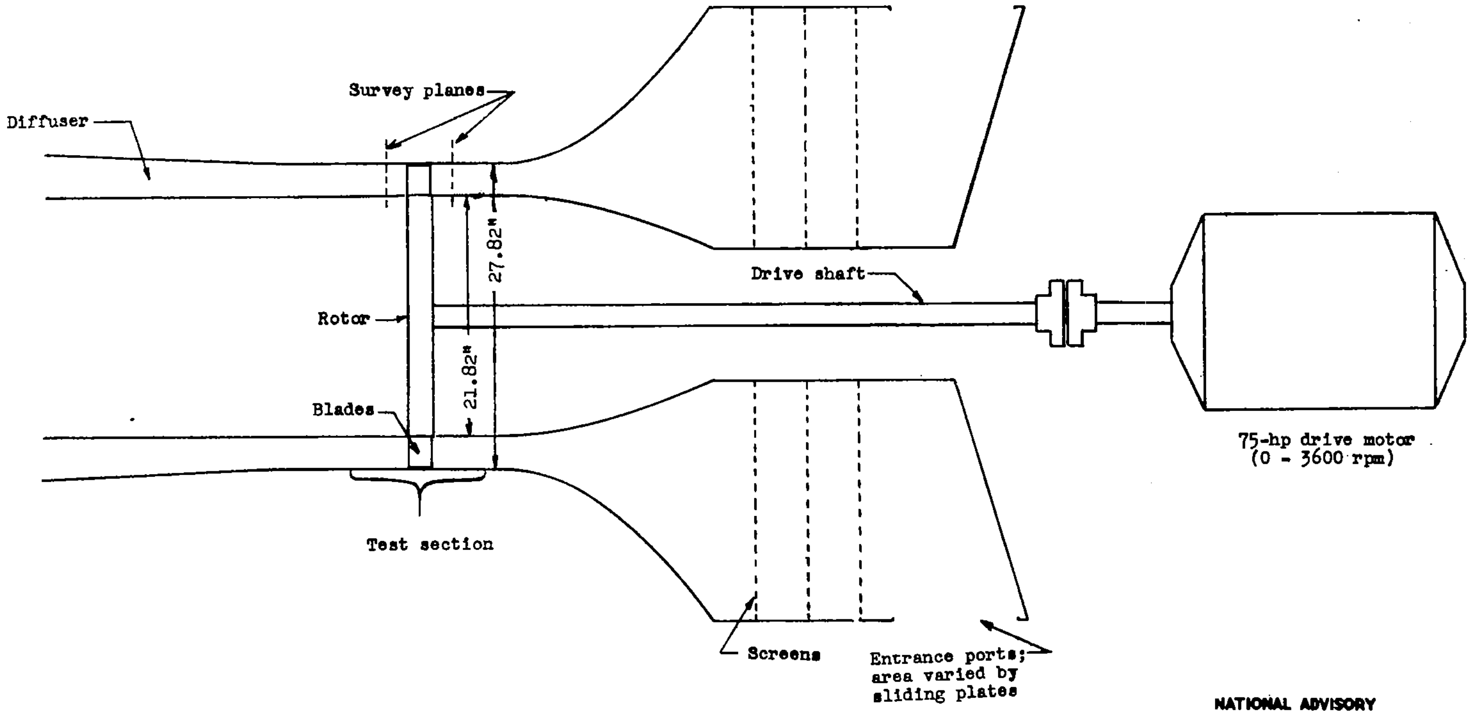

NATIONAL ADVISORY
COMMITTEE FOR AERONAUTICS

Figure 4.- Schematic diagram of single-stage test blower.

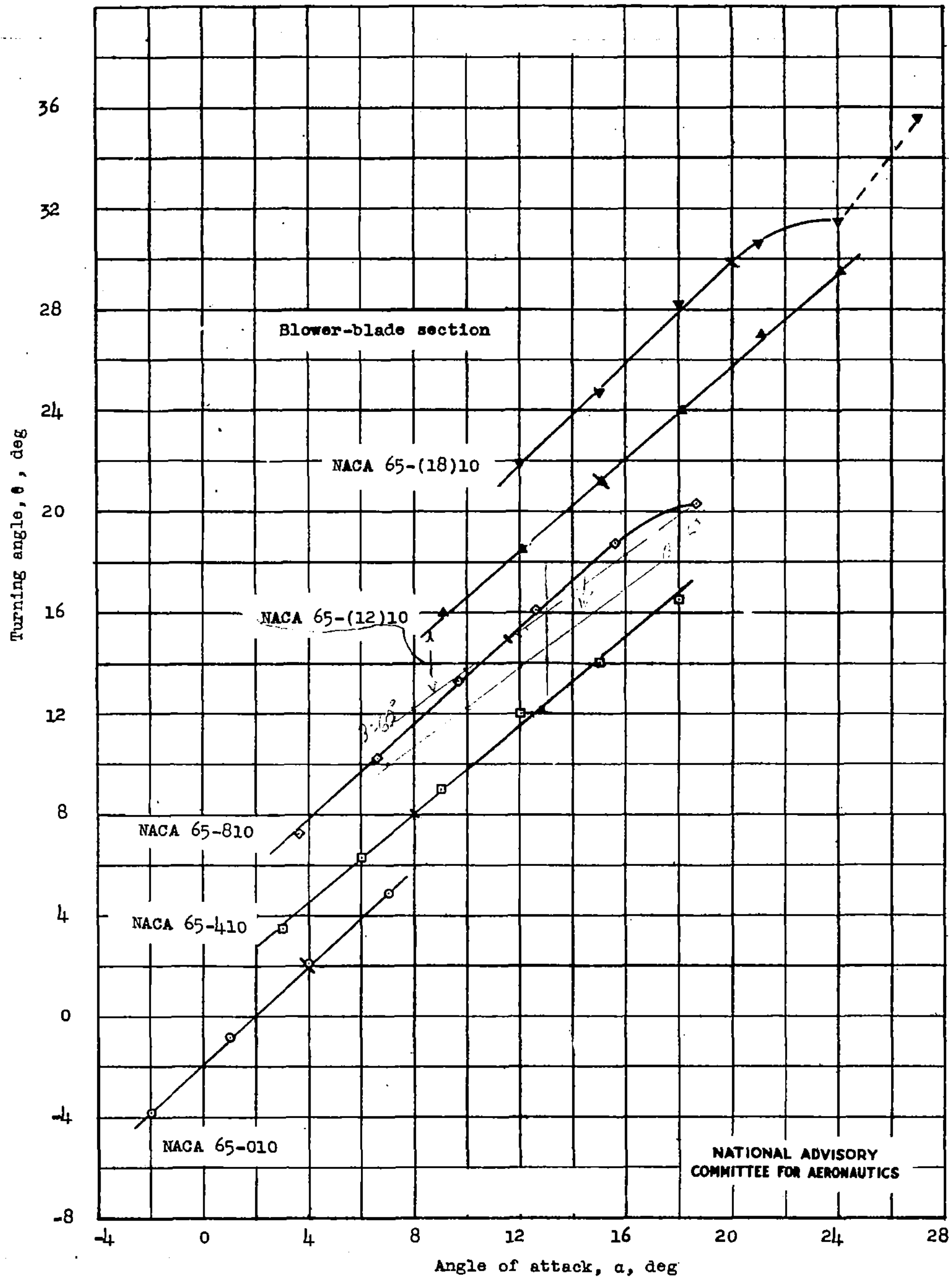

Figure 5.- Turning-angle characteristics; $\beta = 45^{\circ}$; $\sigma = 1.0$. (Short line across curve is design point.)

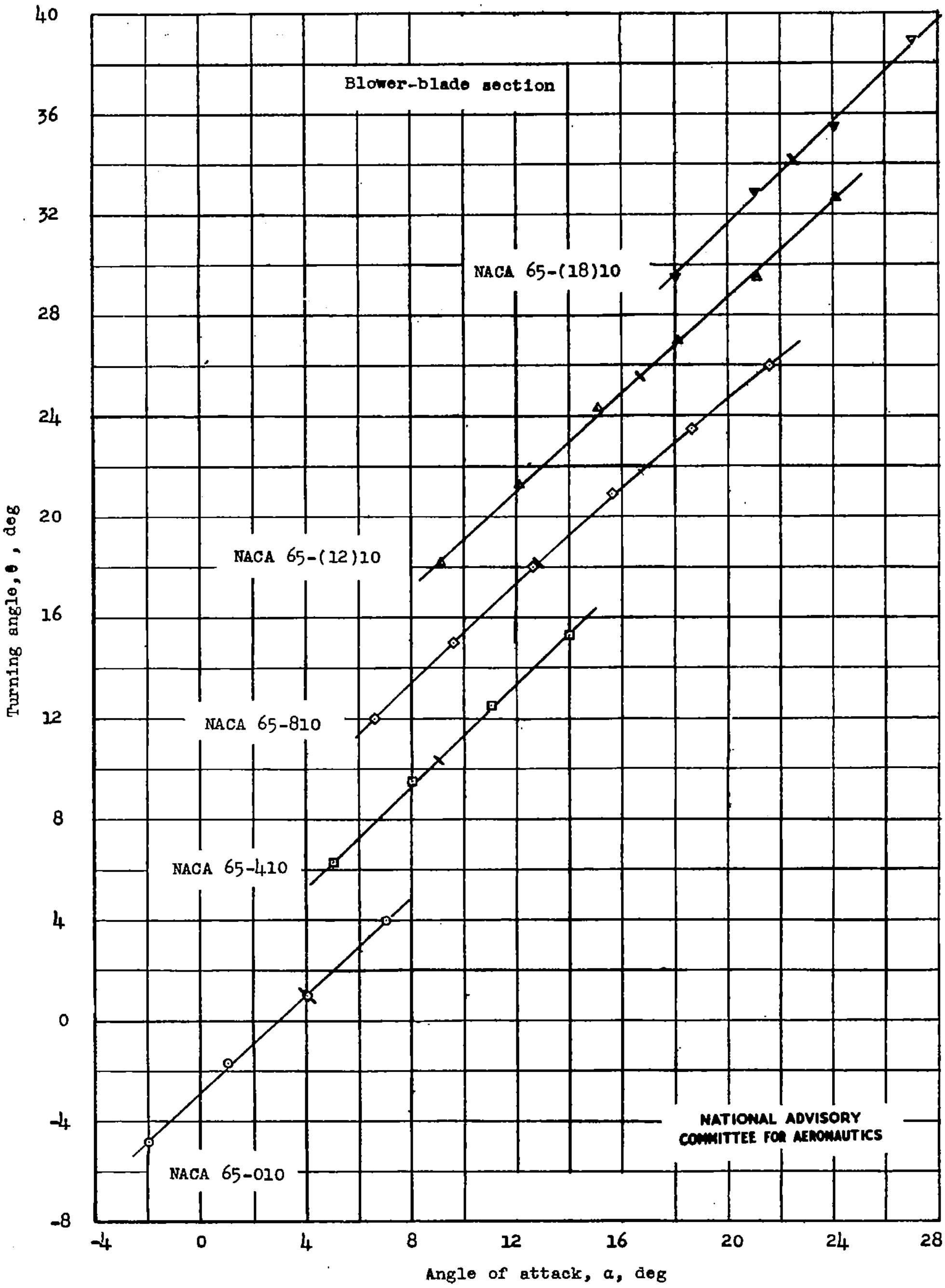

Figure 6.- Turning-angle characteristics; β = 45 ; σ = 1.5. (Short line across curve is design point.)

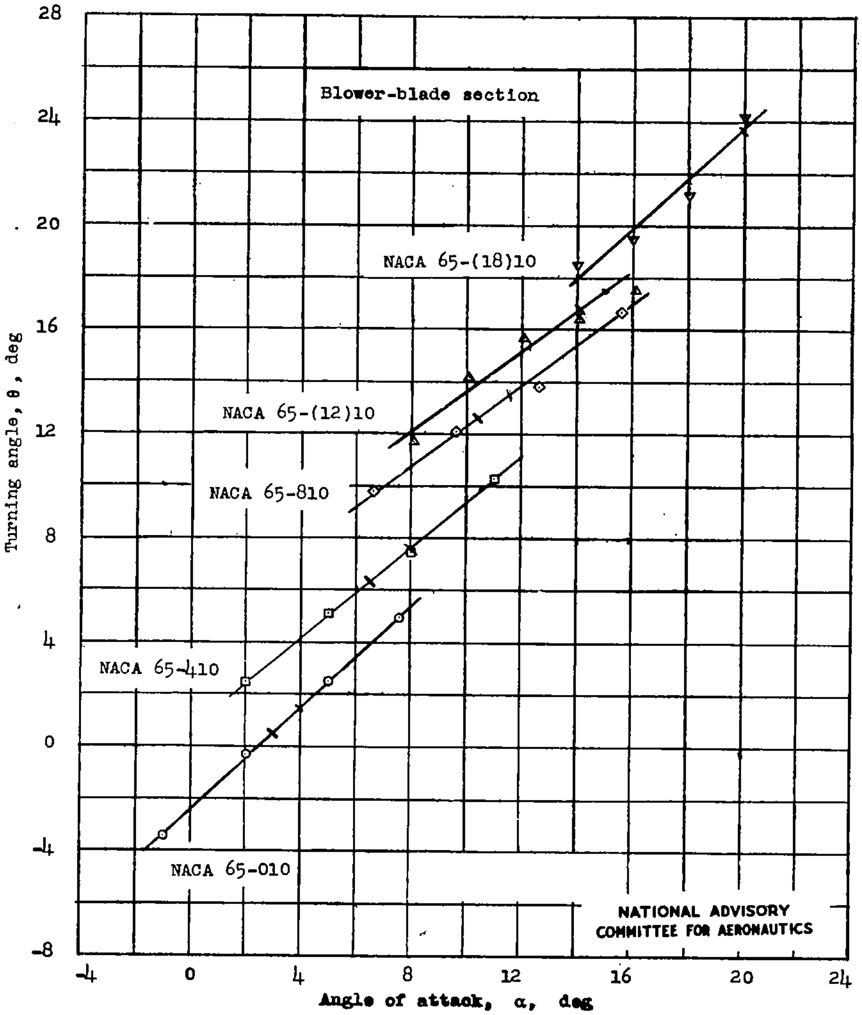

Figure 7.- Turning-angle characteristics; $\beta = 60^{\circ}$; $\sigma = 1.0$. (Short line across curve is design point.)

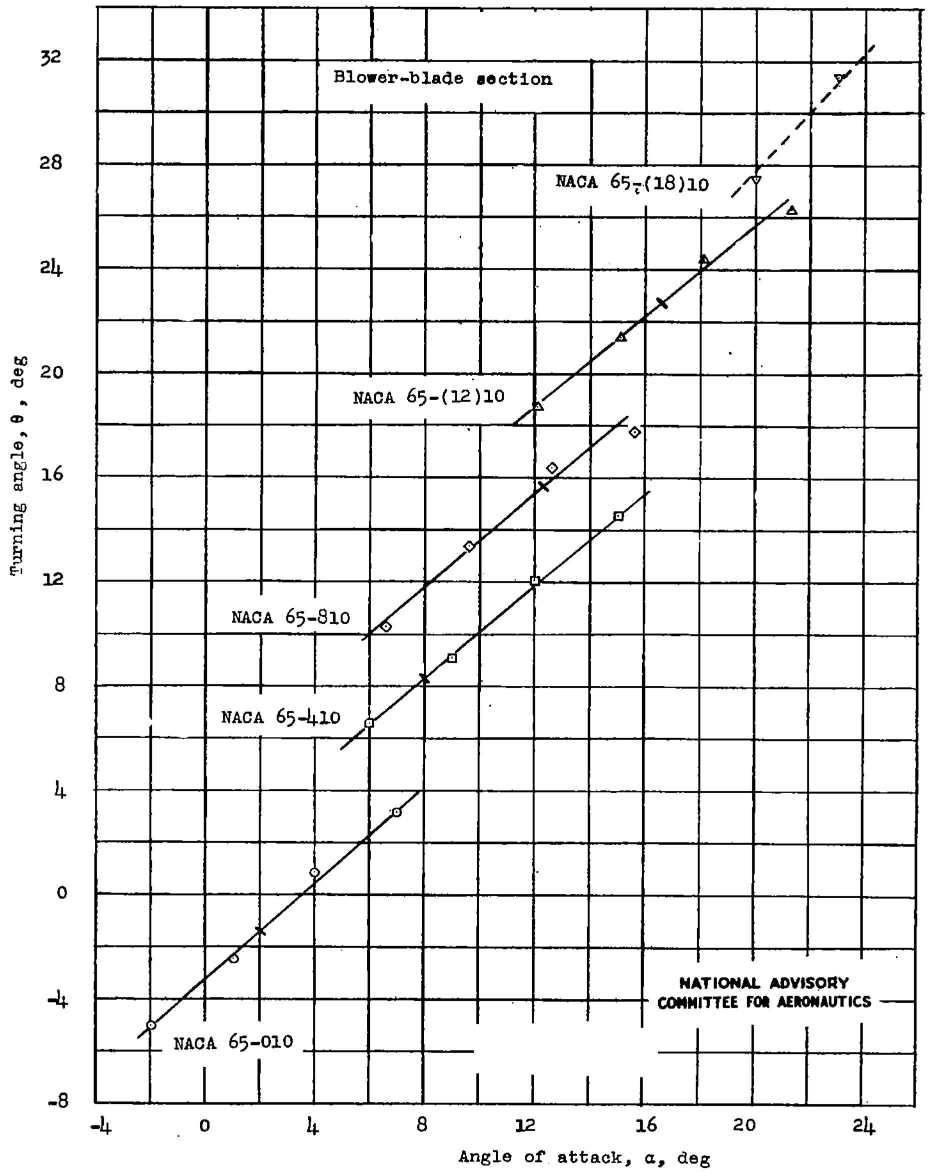

Figure 8.- Turning-angle characteristics; $\beta = 60^{\circ}$; $\sigma = 1.5$. (Short line across curve is design point.)

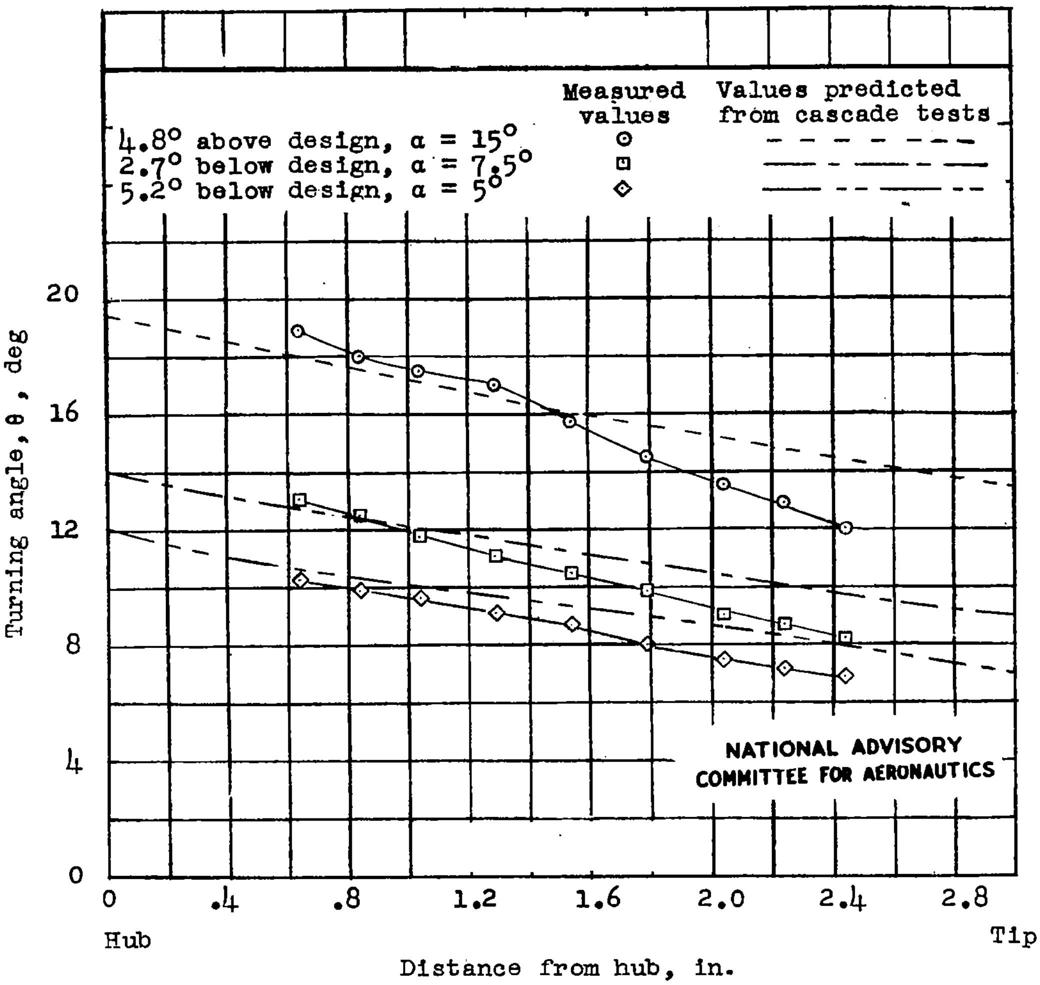

Figure 9.- Variation of turning angle along the blade showing a comparison of measured values from test blower and values predicted from cascade tests.

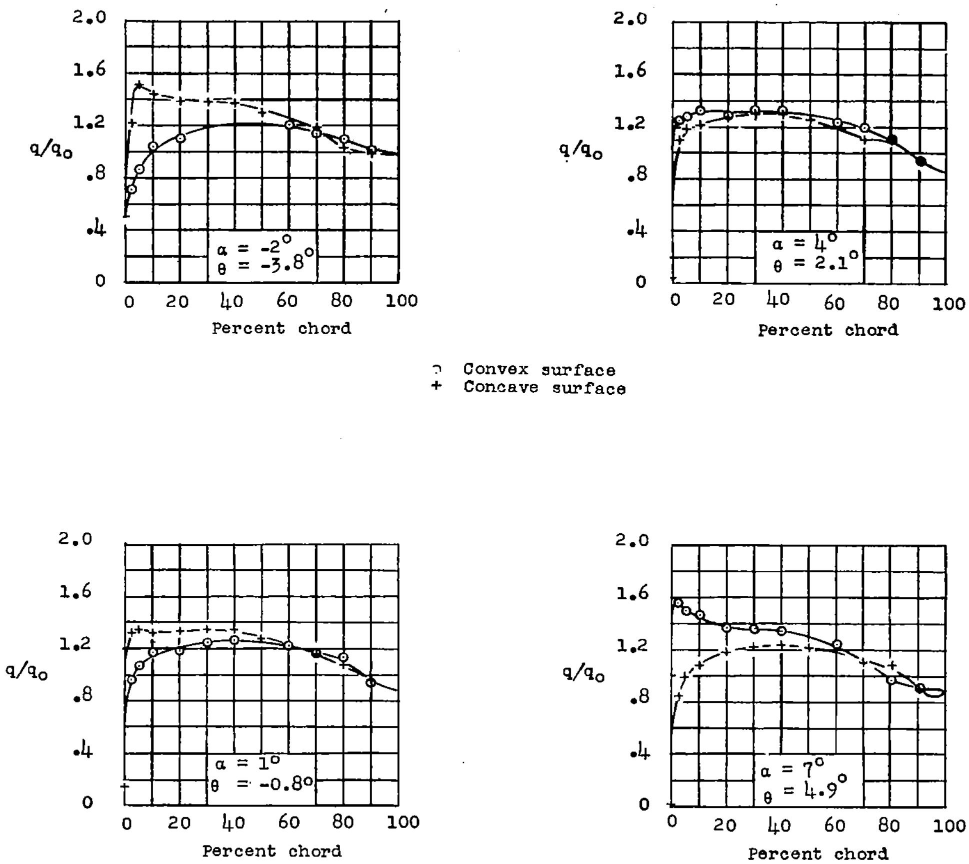

Figure 10.- Section pressure distributions. Cascade of NACA 65-010 blower-blade sections; $\beta = 45^{\circ}$; $\sigma = 1.0$; $\alpha_d = 4.0^{\circ}$.

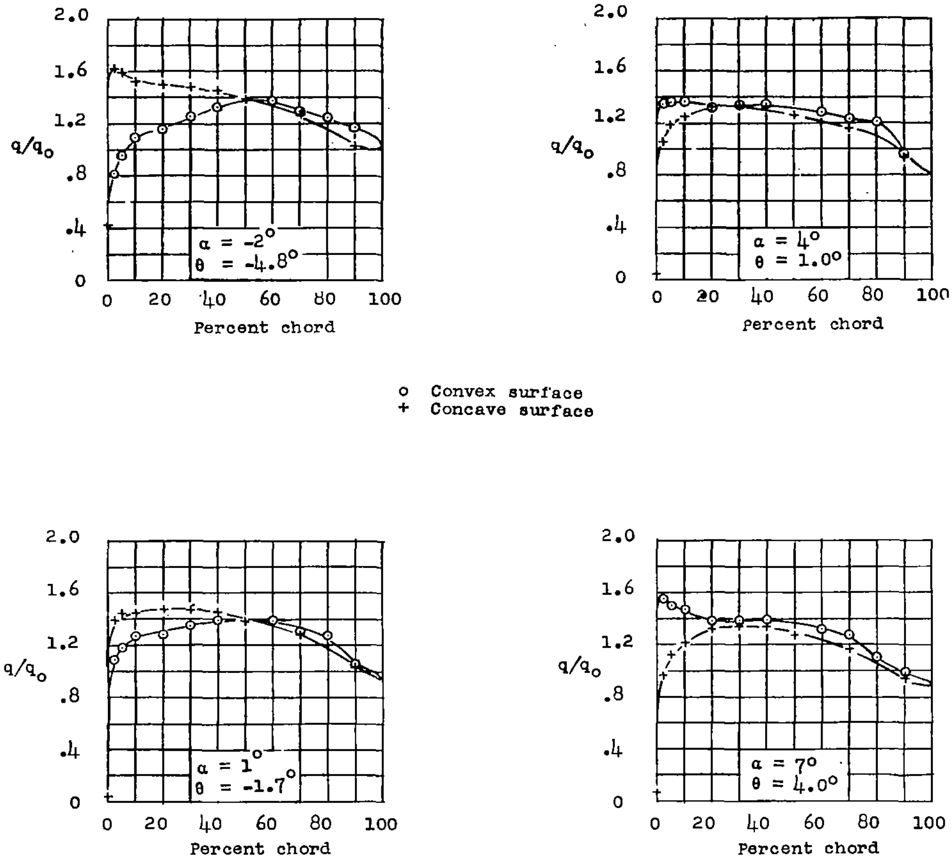

NATIONAL ADVISORY COMMITTEE FOR AERONAUTICS

Figure 11.- Section pressure distributions. Cascade of NACA 65-010 blower-blade sections; $\beta = 45^\circ$; $\sigma = 1.5$; $\alpha_d = 4.0^\circ$.

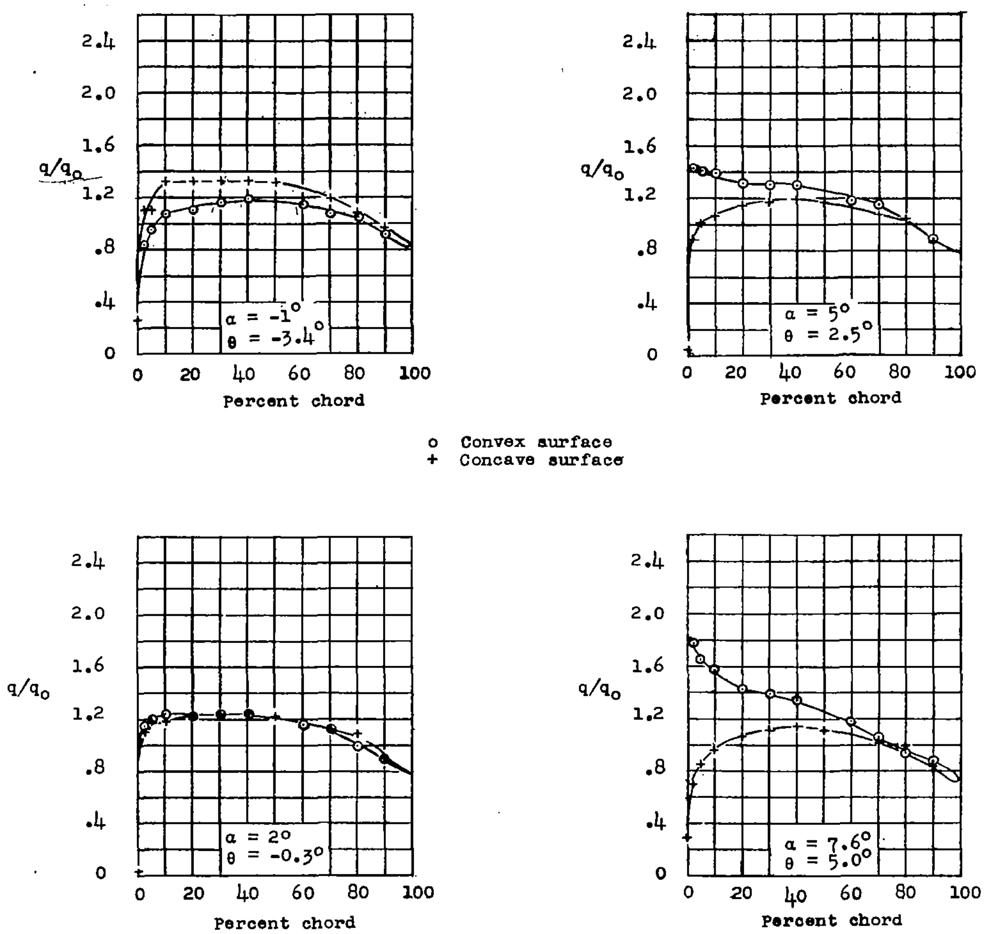

NATIONAL ADVISORY COMMITTEE FOR AERONAUTICS

Figure 12.- Section pressure distributions. Cascade of NACA 65-010 blower-blade sections; $\beta = 60^\circ$; $\sigma = 1.00$; $\alpha_d = 3.0^\circ$.

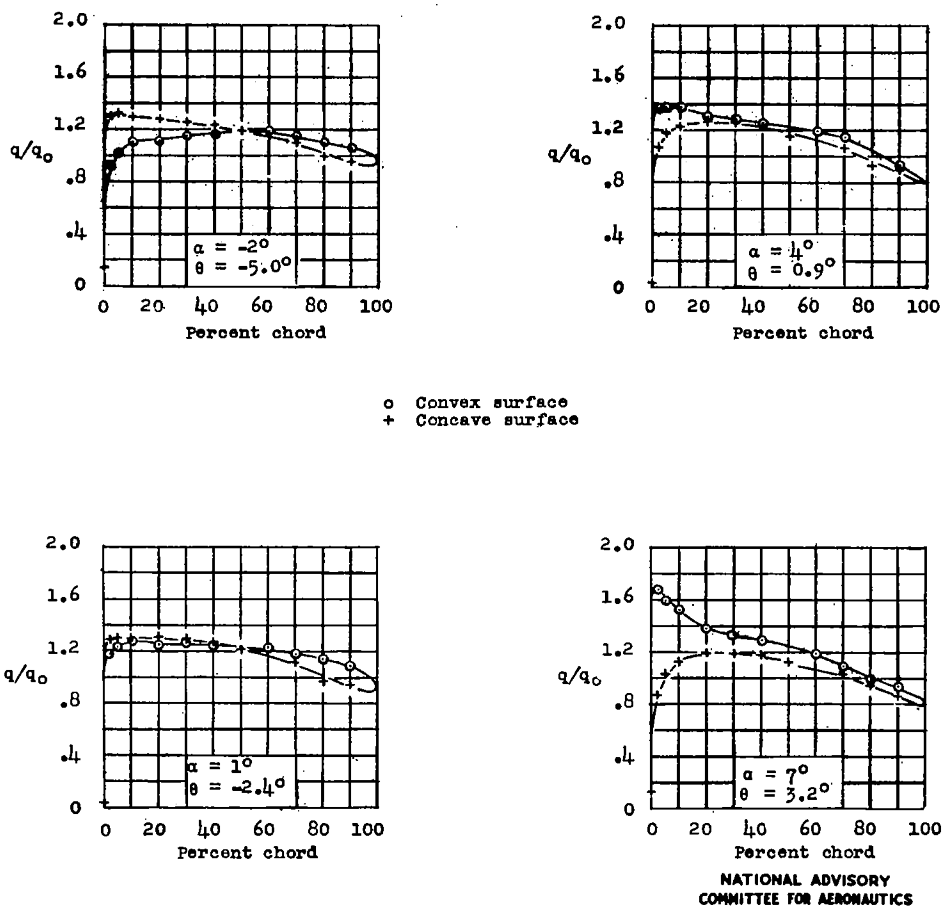

Figure 13.- Section pressure distributions. Cascade of NACA 65-010 blower-blade sections; $\beta = 60^\circ$; $\sigma = 1.5$; $\alpha_d = 2.0^\circ$.

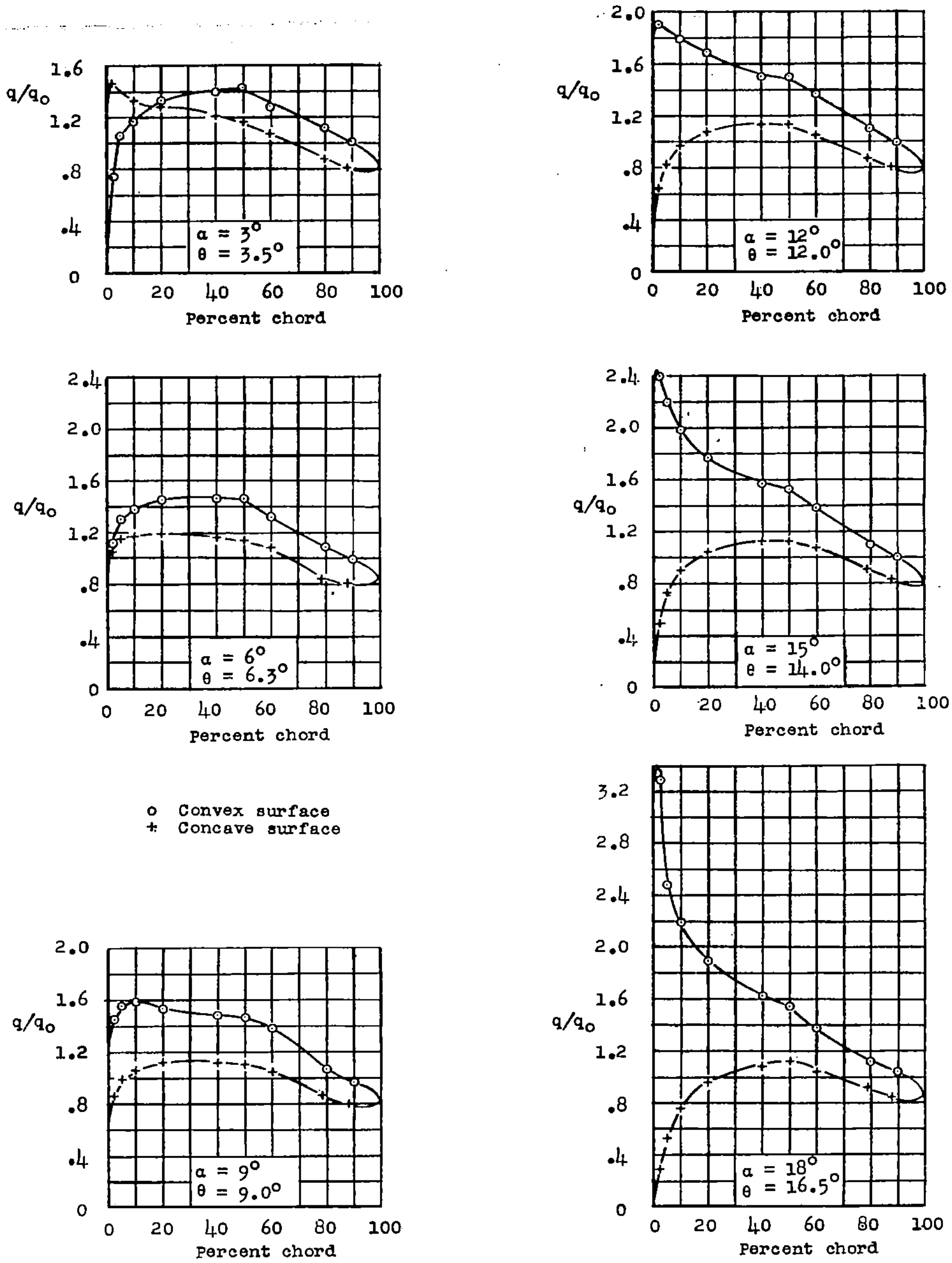

NATIONAL ADVISORY
COMMITTEE FOR AERONAUTICS

Figure 14.- Section pressure distributions. Cascade of NACA 65-410 blower-blade sections; $\beta = 45^{\circ}$; $\sigma = 1.0$; $\alpha_d = 8^{\circ}$.

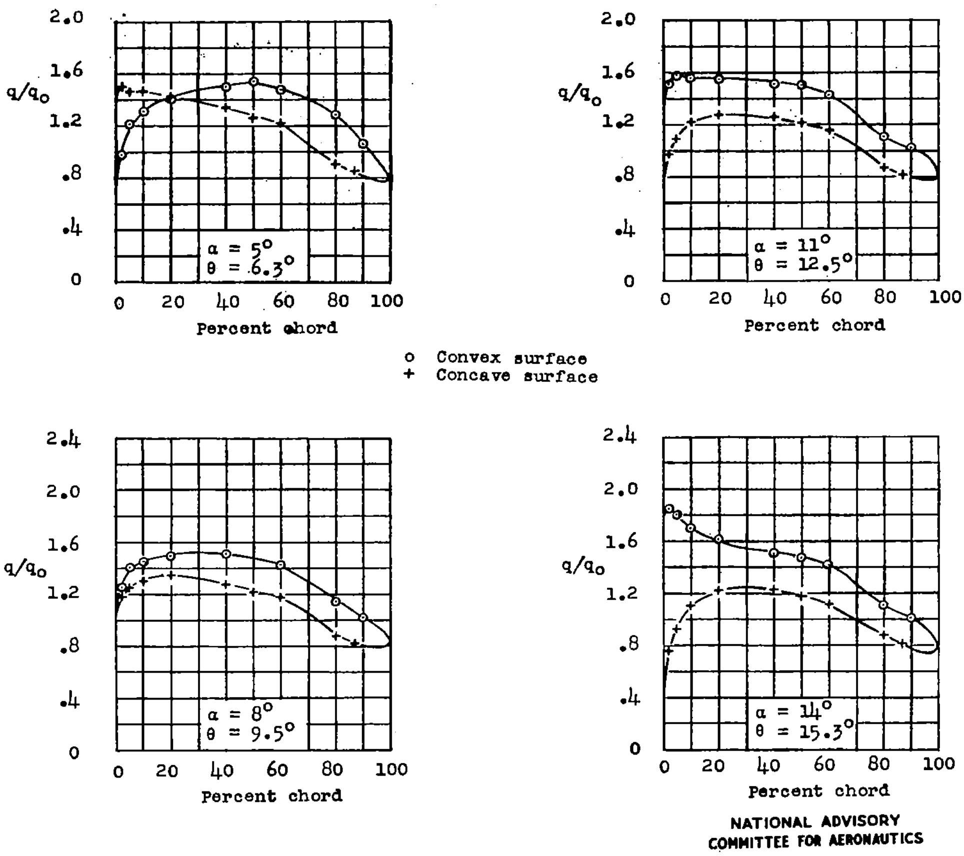

Figure 15.- Section pressure distributions. Cascade of NACA 65-410 blower-blade sections; $\beta = 45^\circ$; $\sigma = 1.5$; $\alpha_d = 9.0^\circ$.

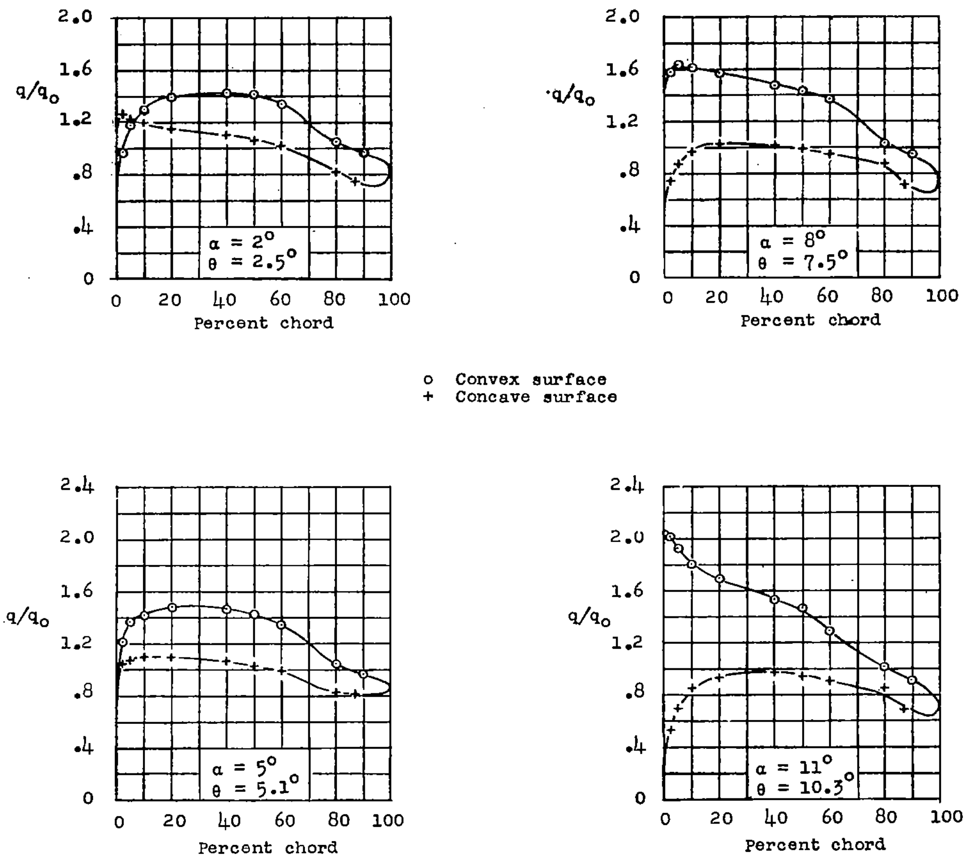

NATIONAL ADVISORY COMMITTEE FOR AERONAUTICS

Figure 16.- Section pressure distributions. Cascade of NACA 65-410 blower-blade sections; $\beta = 60^o$; $\sigma = 1.0$; $\alpha_d = 6.5^o$.

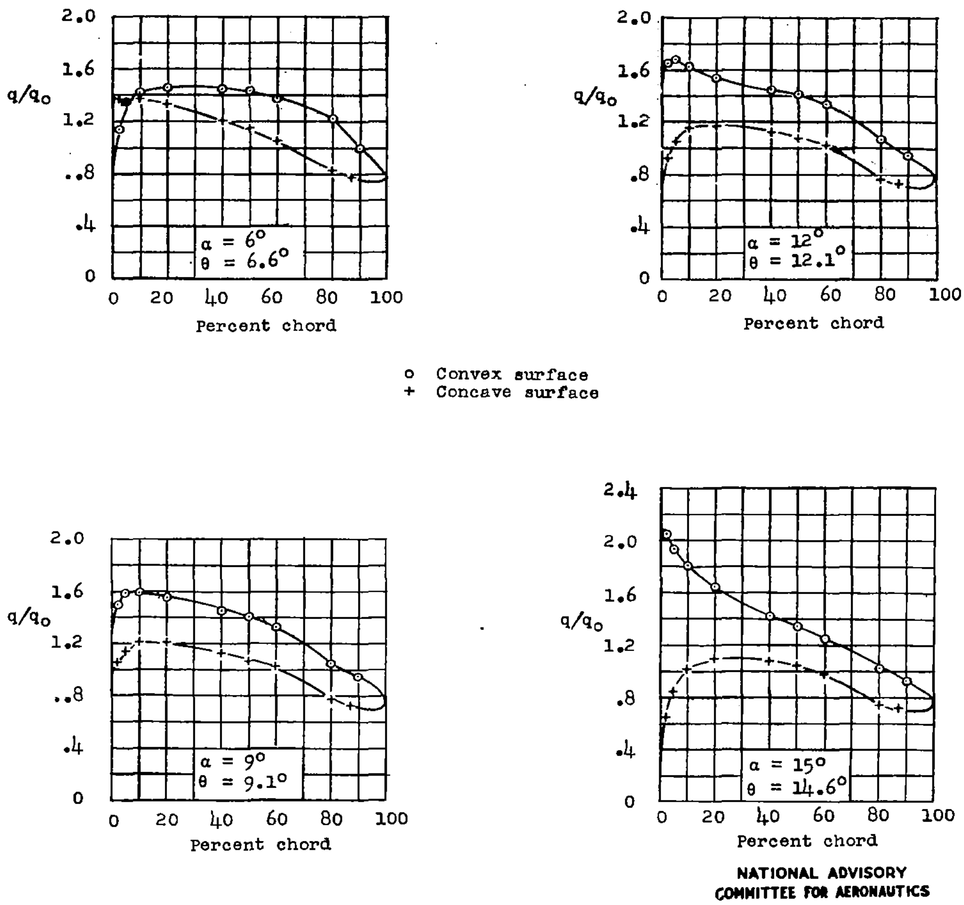

Figure 17.- Section pressure distributions. Cascade of NACA 65-410 blower-blade sections; $\beta = 60^{\circ}$; $\sigma = 1.5$; $\alpha_d = 8.0^{\circ}$.

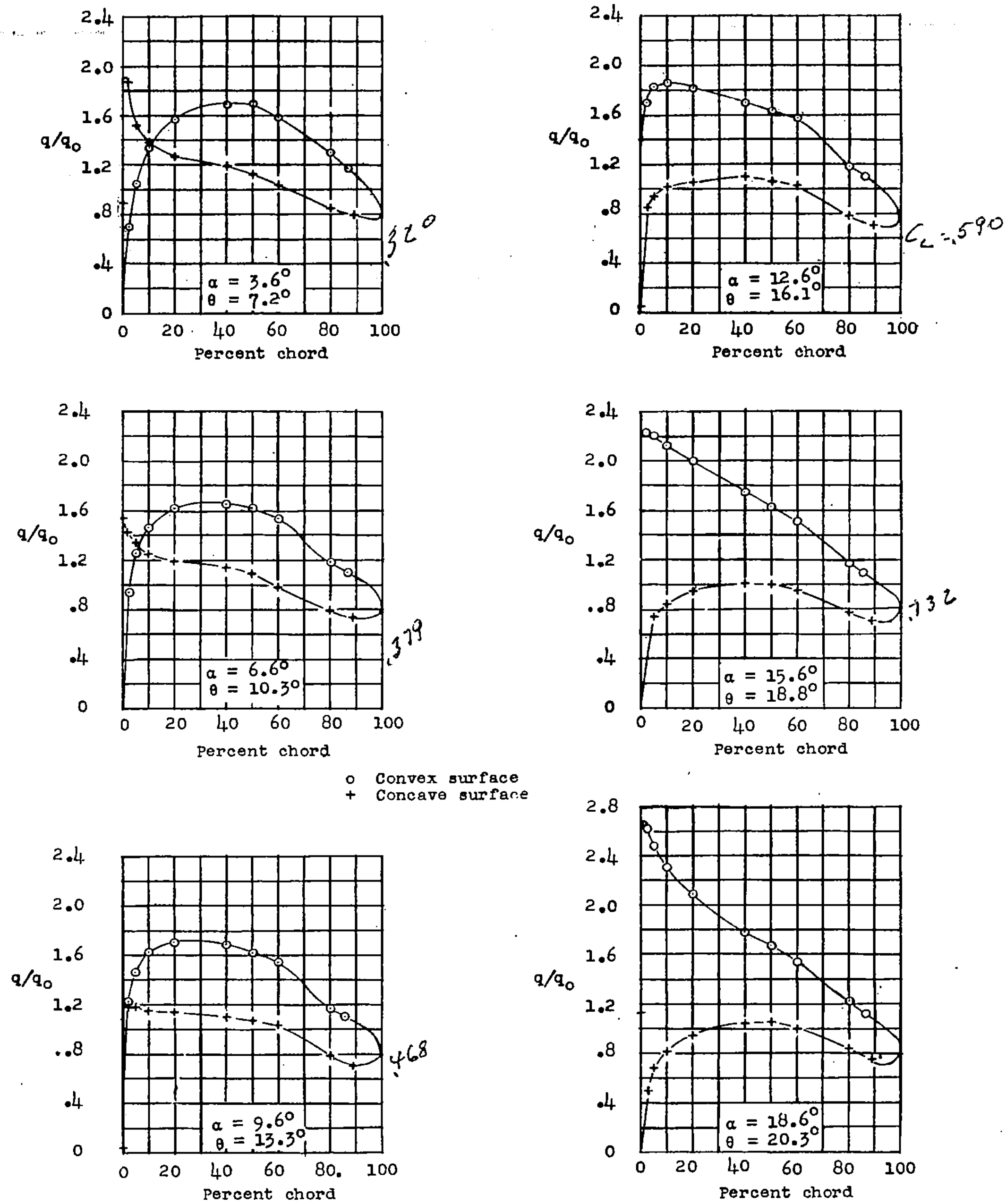

NATIONAL ADVISORY COMMITTEE FOR AERONAUTICS

Figure 18.- Section pressure distributions. Cascade of NACA 65-810 blower-blade sections; $\beta = 45°$; $\sigma = 1.0$; $\alpha_d = 11.5°$.

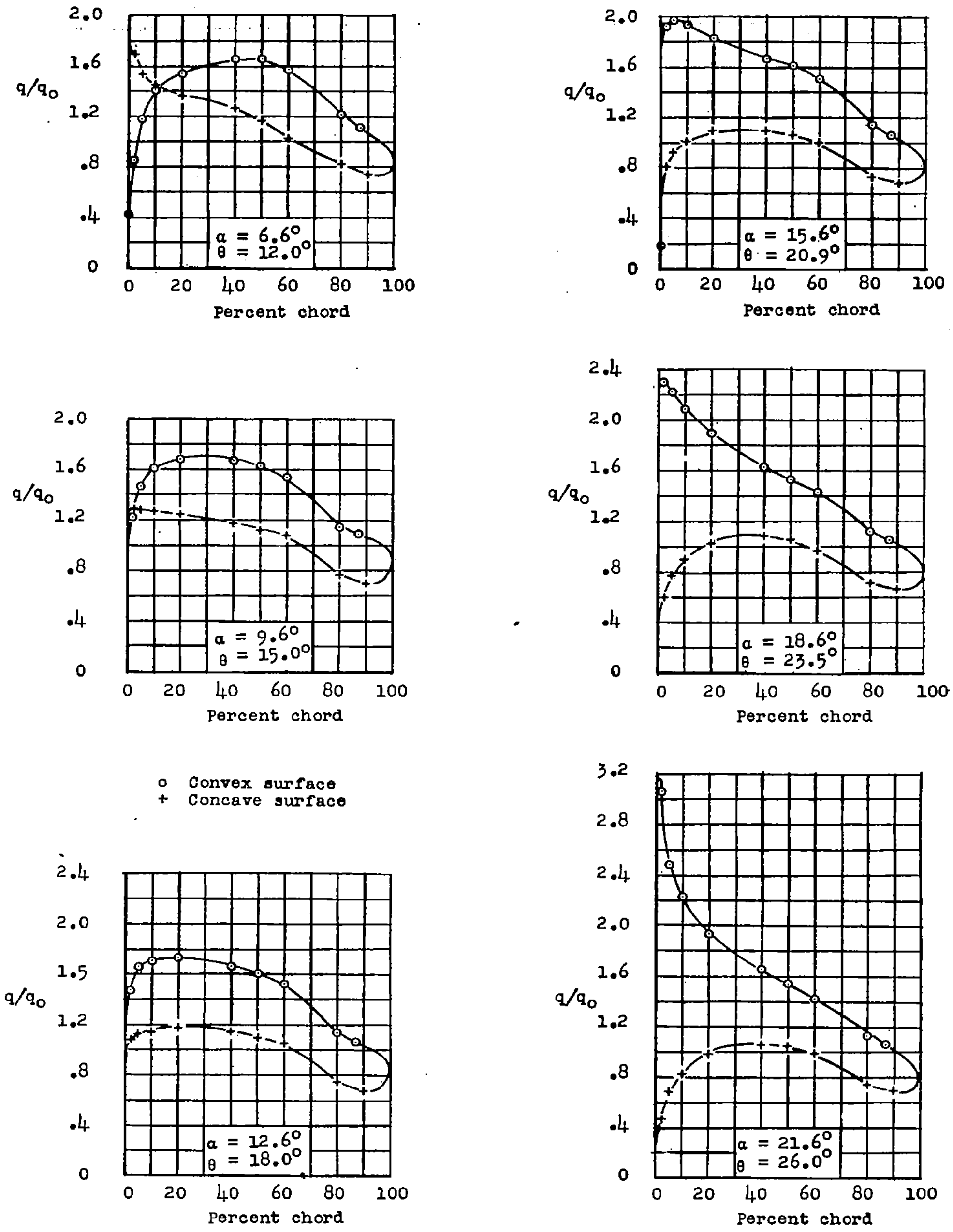

NATIONAL ADVISORY
COMMITTEE FOR AERONAUTICS

Figure 19.- Section pressure distributions. Cascade of NACA 65-810 blower-blade sections; $\beta = 45^\circ$; $\sigma = 1.5$; $\alpha_d = 12.8^\circ$.

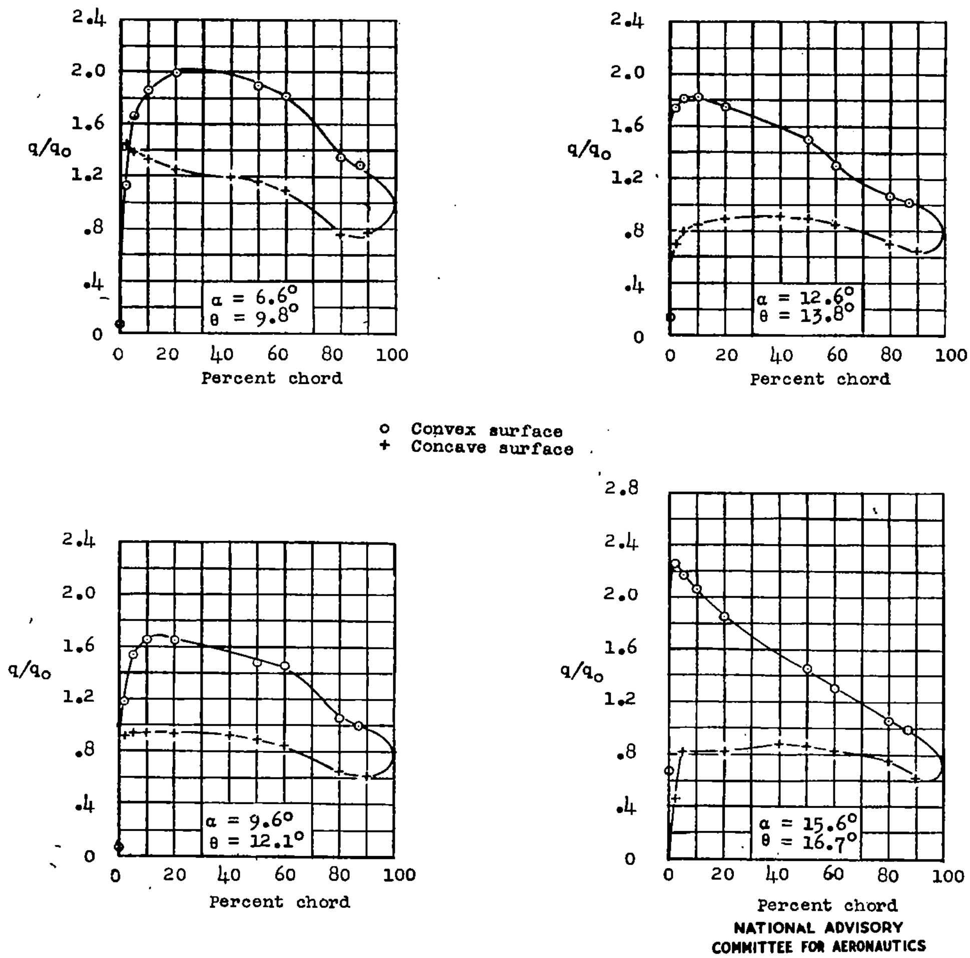

Figure 20.- Section pressure distributions. Cascade of NACA 65-810 blower-blade sections; $\beta = 60^\circ$; $\sigma = 1.0$; $\alpha_d = 10.2^\circ$.

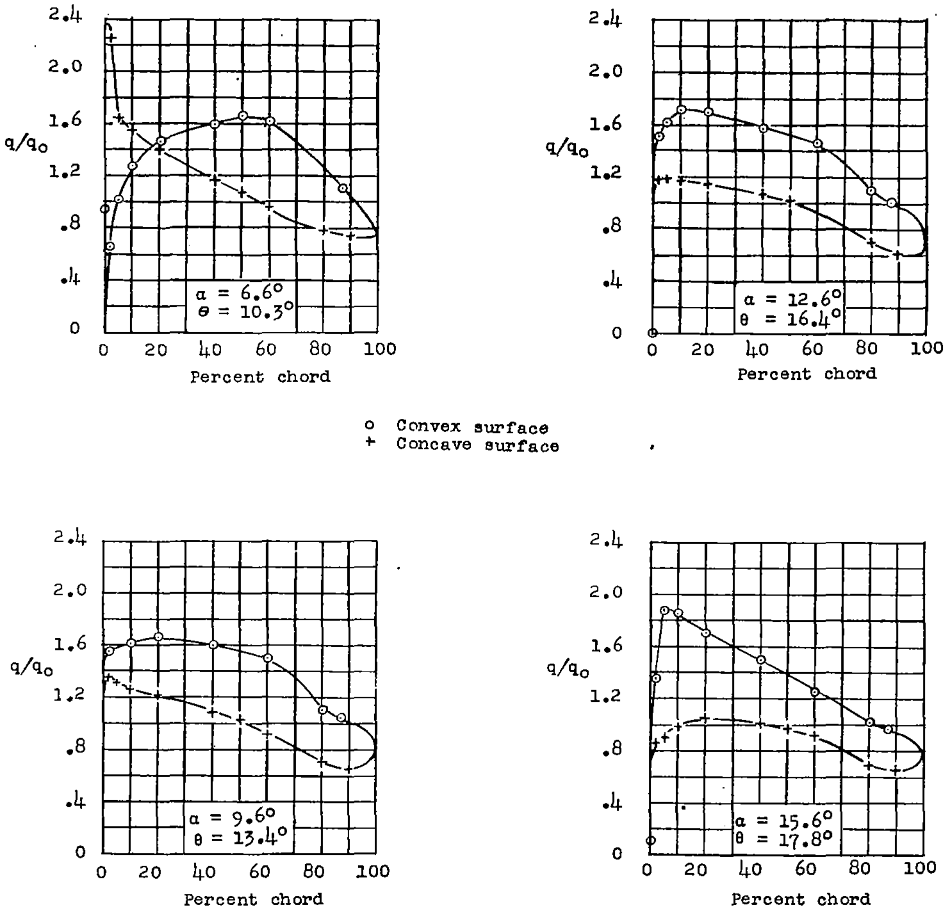

NATIONAL ADVISORY
COMMITTEE FOR AERONAUTICS

Figure 21.- Section pressure distributions. Cascade of NACA 65-810 blower-blade sections; $\beta = 60^{\circ}$; $\sigma = 1.5$; $\alpha_d = 12.3^{\circ}$.

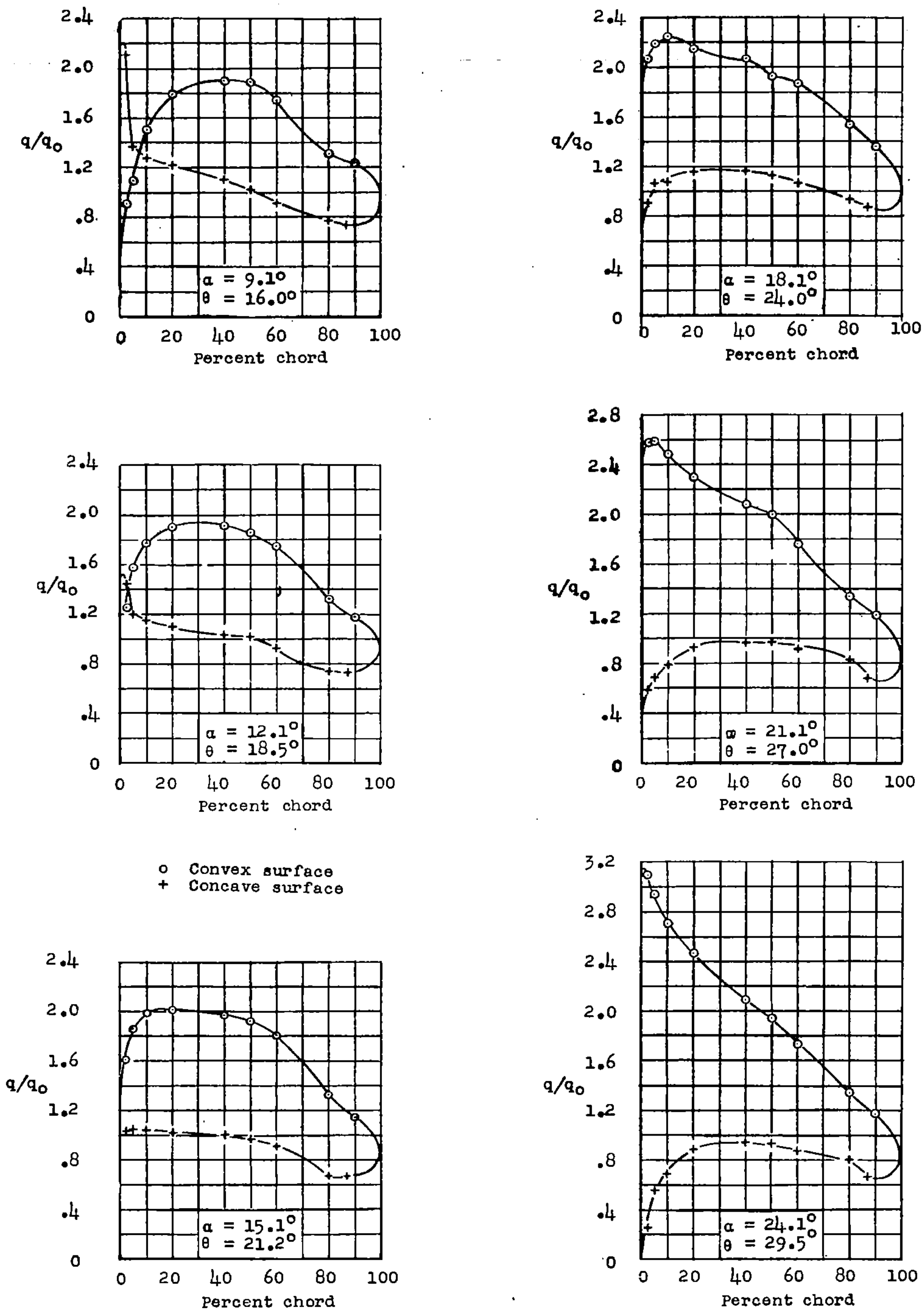

NATIONAL ADVISORY
COMMITTEE FOR AERONAUTICS

Figure 22.- Section pressure distributions. Cascade of NACA 65-(12)10 blower-blade sections; $\beta = 45^{\circ}$; $\sigma = 1.0$; $\alpha_d = 15.0^{\circ}$.

Isolated airfoil $\alpha_{cl} = 4^{\circ}$; $C_L = 1.02$

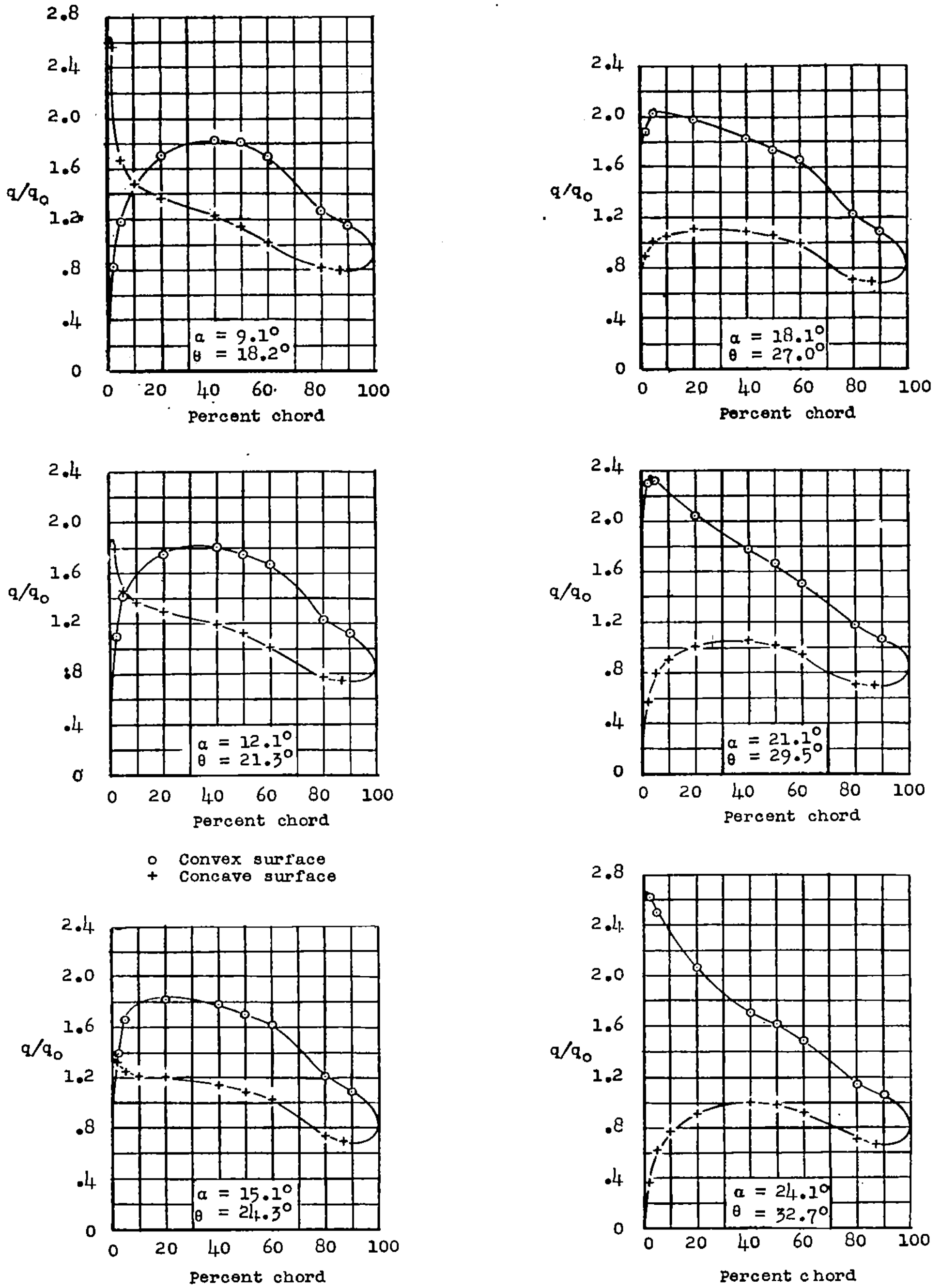

NATIONAL ADVISORY COMMITTEE FOR AERONAUTICS

Figure 23.- Section pressure distributions. Cascade of NACA 65-(12)10 blower-blade sections; $\beta = 45°$; $\sigma = 1.5$; $\alpha_d = 16.7°$.

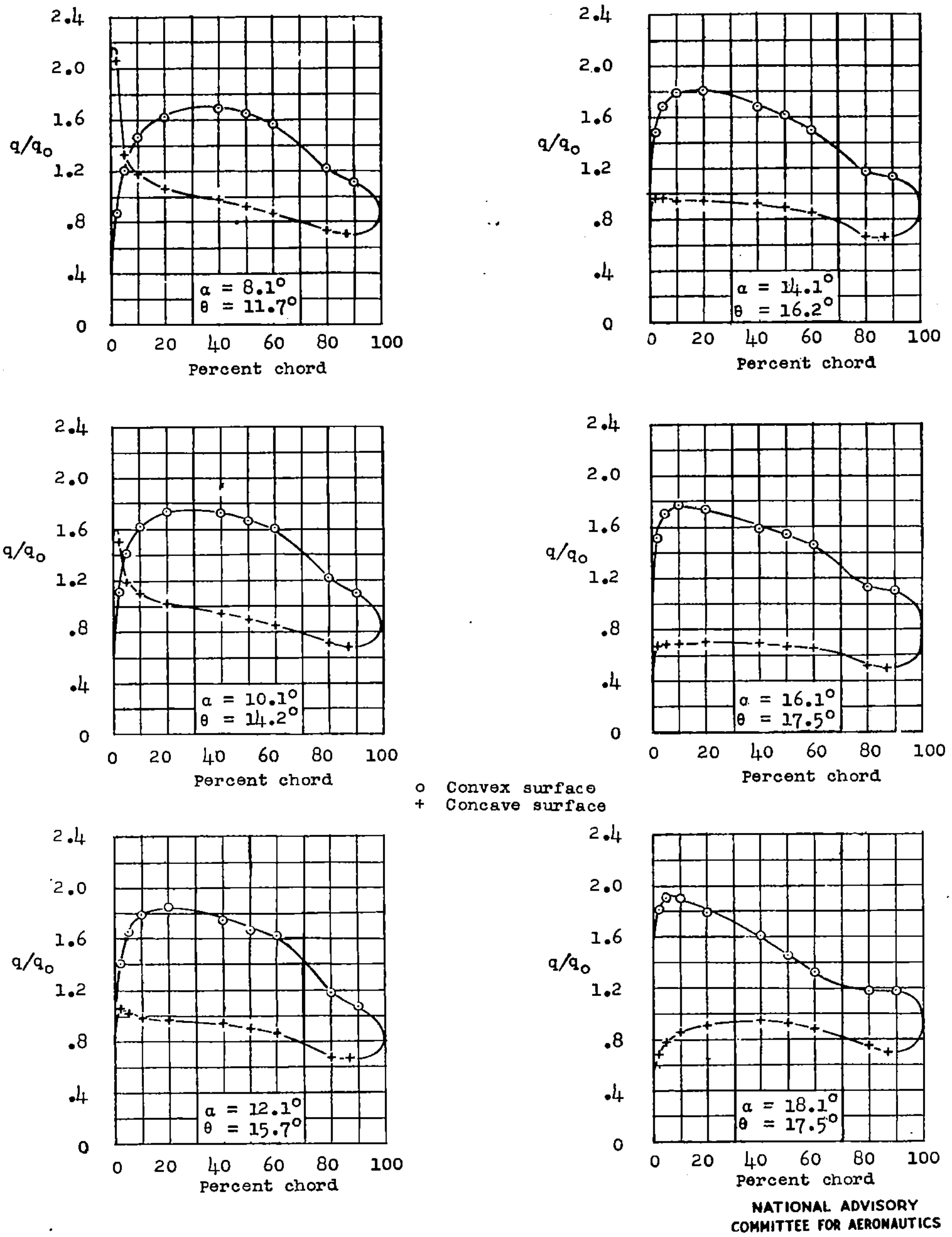

Figure 24.- Section pressure distributions. Cascade of NACA 65-(12)10 blower-blade sections; $\beta = 60^{\circ}$; $\sigma = 1$; $\alpha_d = 14.1^{\circ}$.

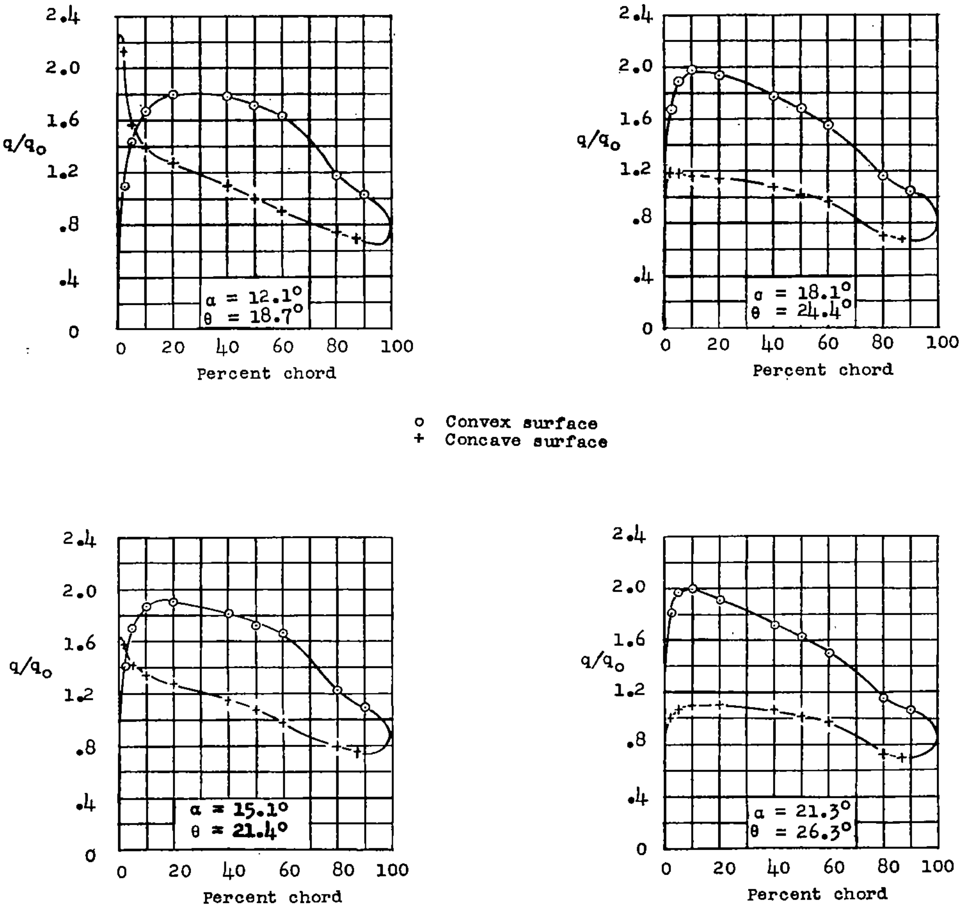

NATIONAL ADVISORY
COMMITTEE FOR AERONAUTICS

Figure 25.- Section pressure distributions. Cascade of NACA 65-(12)10 blower-blade sections; $\beta = 60°$; $\sigma = 1.5$; $\alpha_d = 16.6°$.

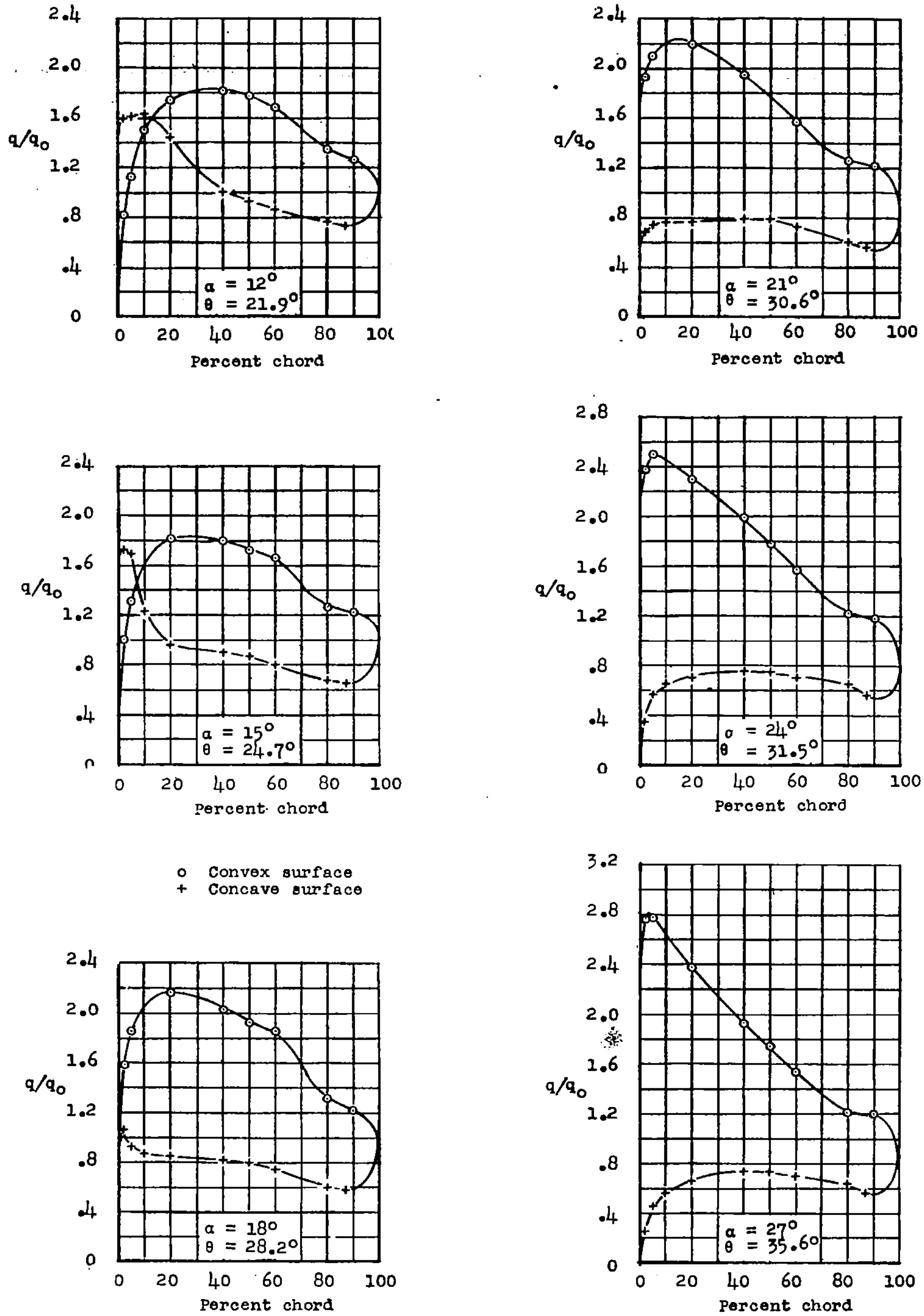

NATIONAL ADVISORY COMMITTEE FOR AERONAUTICS

Figure 26.- Section pressure distributions. Cascade of NACA 65-(18)10 blower-blade sections; $\beta = 45^{\circ}$; $\sigma = 1.0$; $\alpha_d = 20.0^{\circ}$.

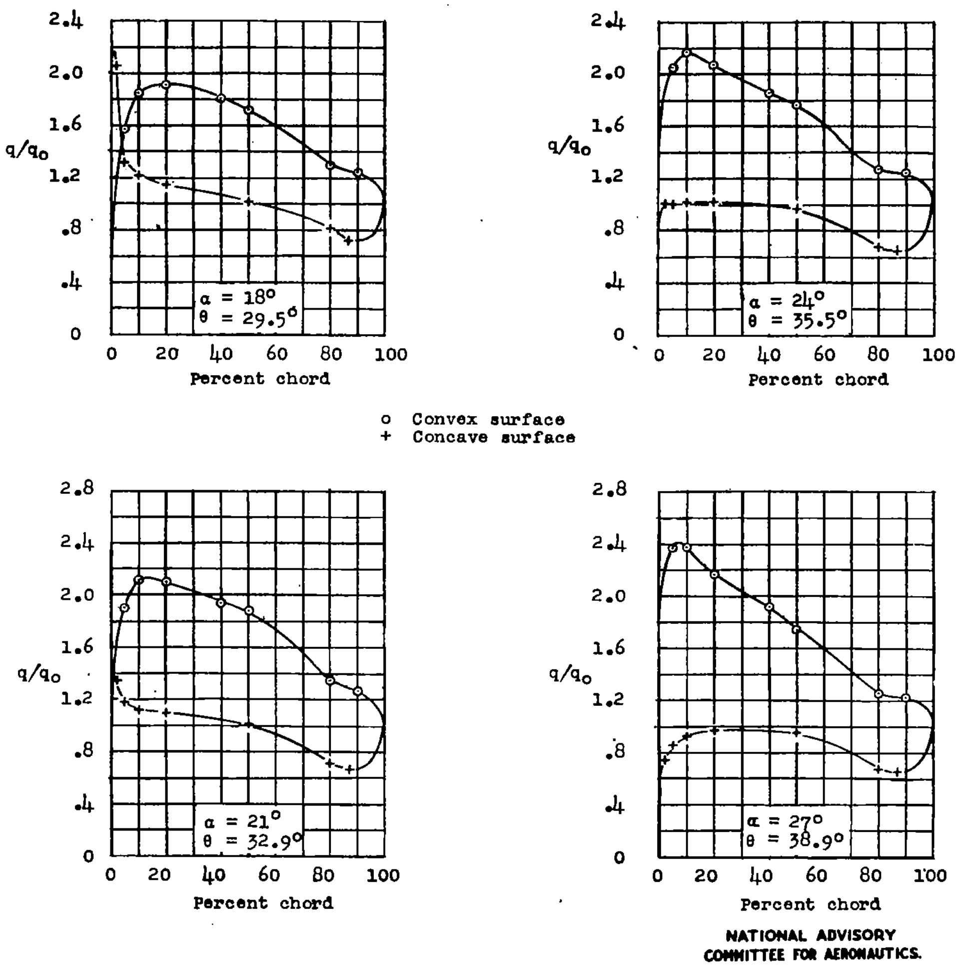

Figure 27.- Section pressure distributions. Cascade of NACA 65-(18)10 blower-blade sections; $\beta = 45^{\circ}$; $\sigma = 1.5$; $\alpha_d = 22.5^{\circ}$.

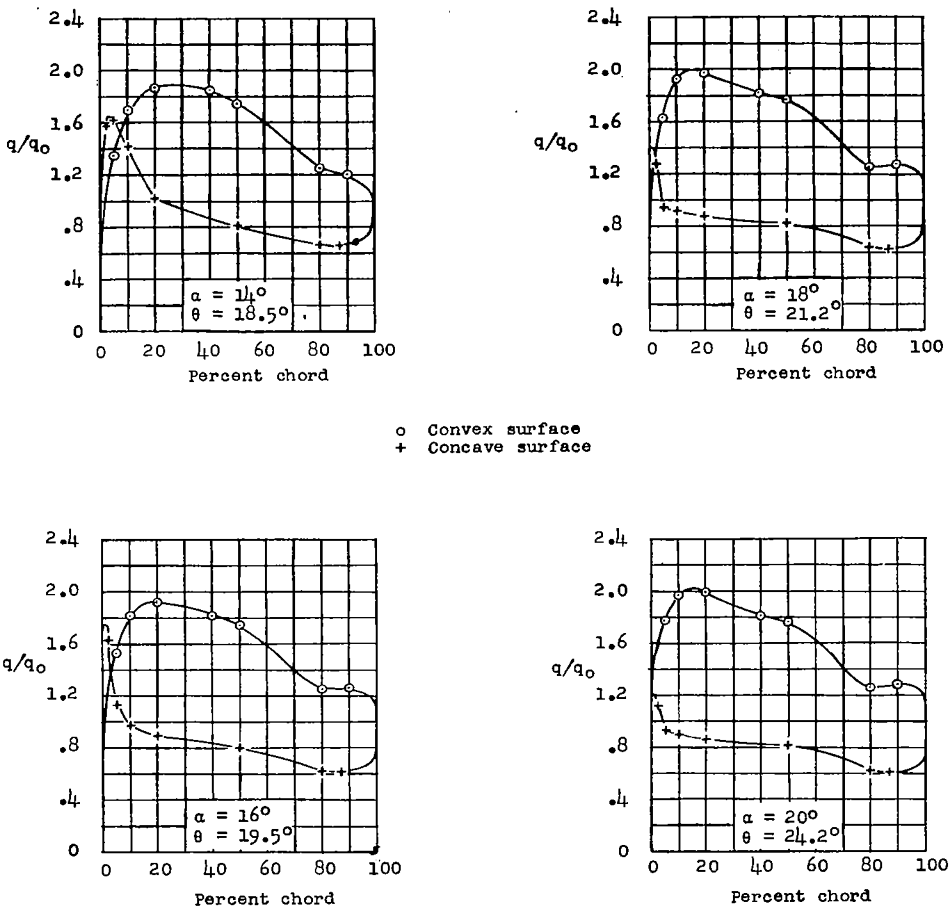

NATIONAL ADVISORY
COMMITTEE FOR AERONAUTICS

Figure 28.- Section pressure distributions. Cascade of NACA 65-(18)10 blower-blade sections; $\beta = 60°$; $\sigma = 1.0$; no φ_d.

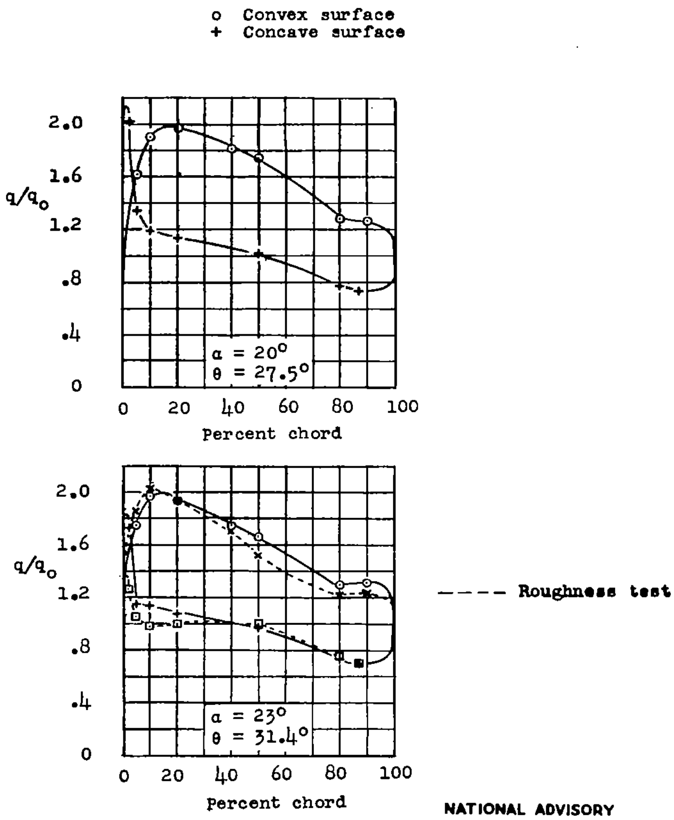

NATIONAL ADVISORY COMMITTEE FOR AERONAUTICS

Figure 29.- Section pressure distributions. Cascade of NACA 65-(18)10 blower-blade sections; $\beta = 60^{\circ}$; $\sigma = 1.5$; no α_d.

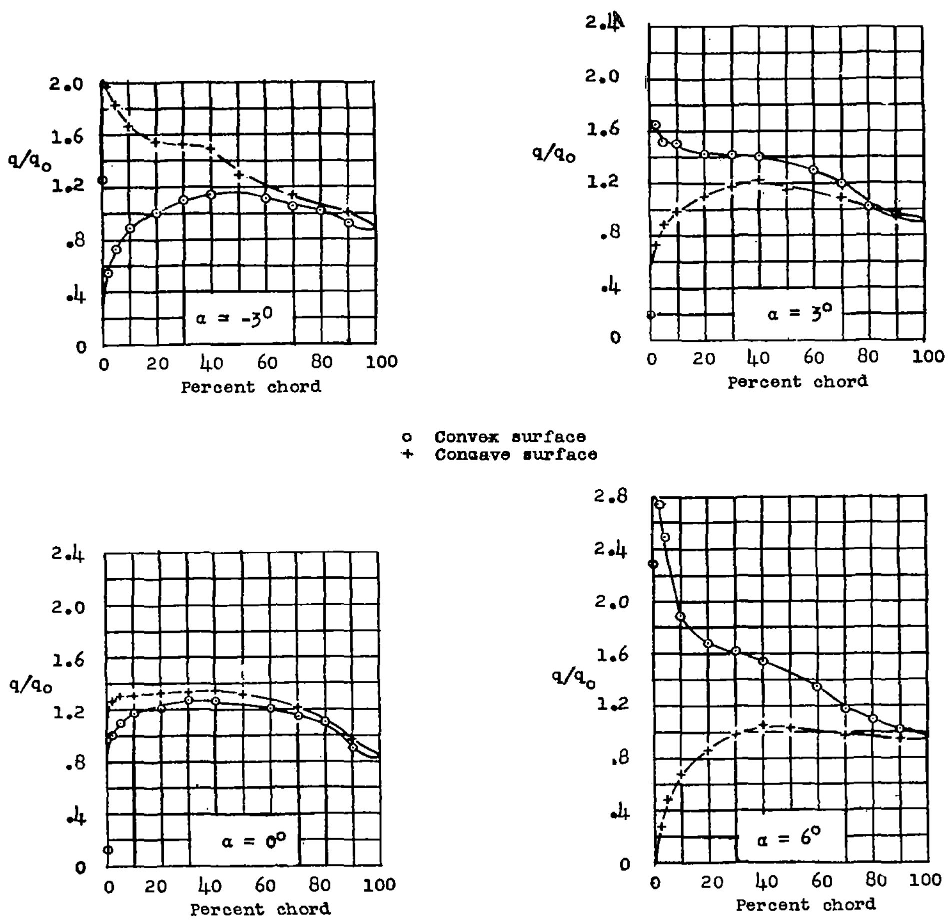

NATIONAL ADVISORY
COMMITTEE FOR AERONAUTICS

Figure 30.- Section pressure distributions. Isolated NACA 65-010 blower-blade section; α_d = .5°.

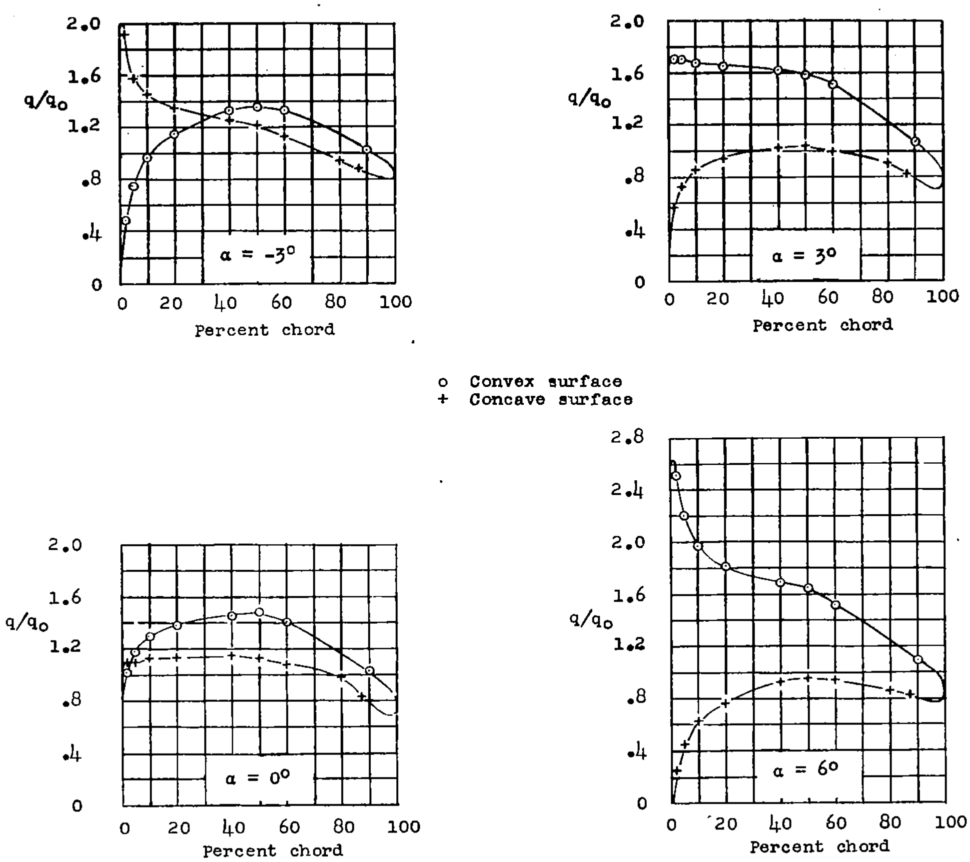

NATIONAL ADVISORY COMMITTEE FOR AERONAUTICS

Figure 31.- Section pressure distributions. Isolated NACA 65-410 blower-blade section; α_d = 2°.

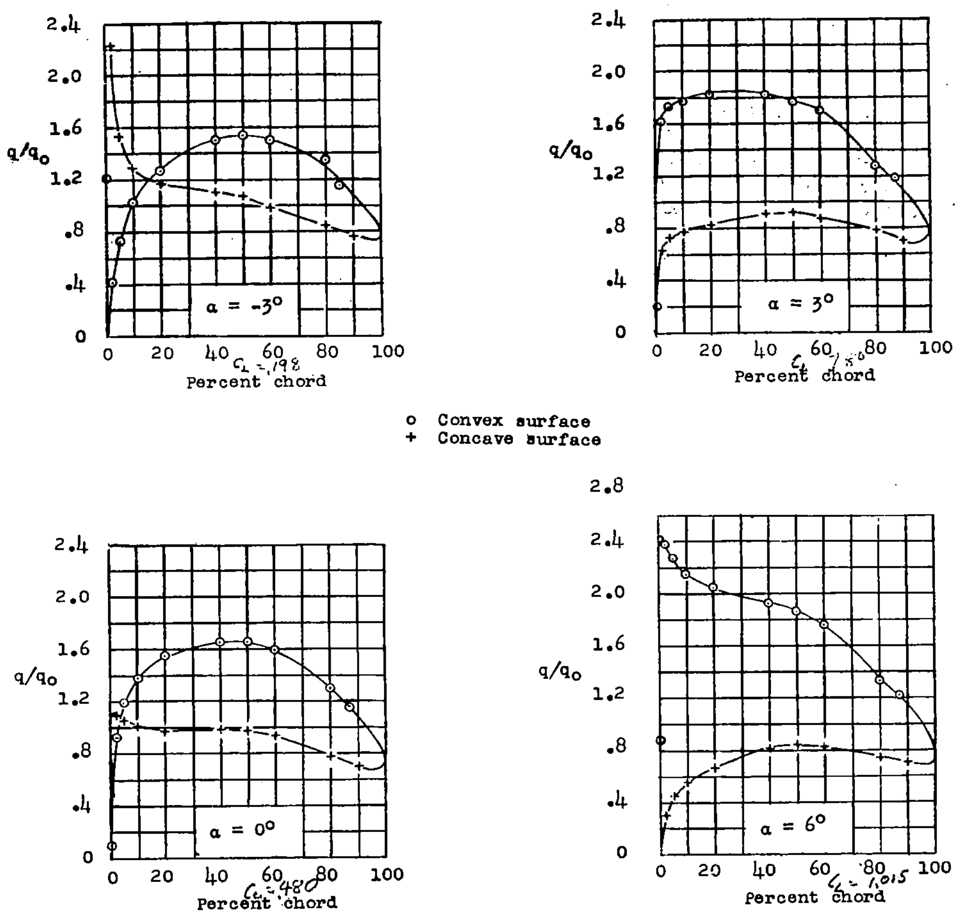

NATIONAL ADVISORY COMMITTEE FOR AERONAUTICS

Figure 32.- Section pressure distributions. Isolated NACA 65-810 blower-blade section; $\alpha_d = 3^\circ$.

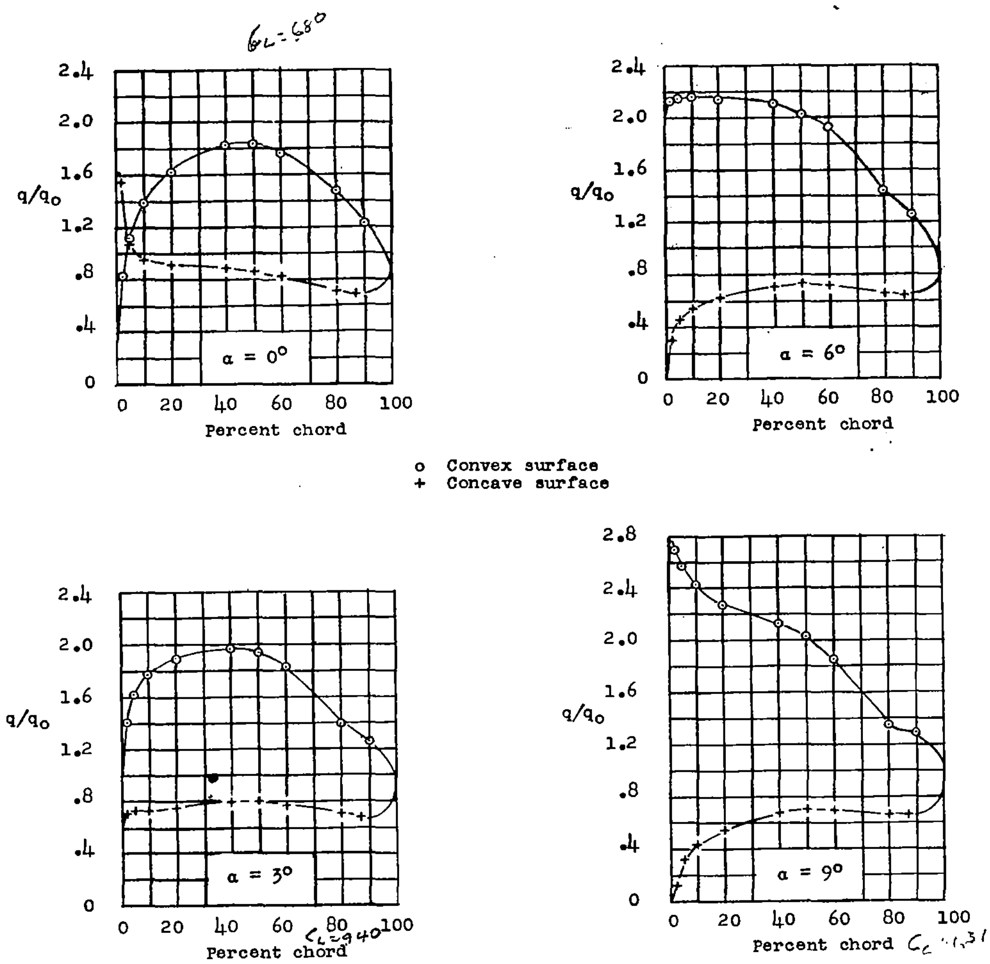

Figure 33.- Section pressure distributions. Isolated NACA 65-(12)10 blower-blade section; $\alpha_d = 4°$.

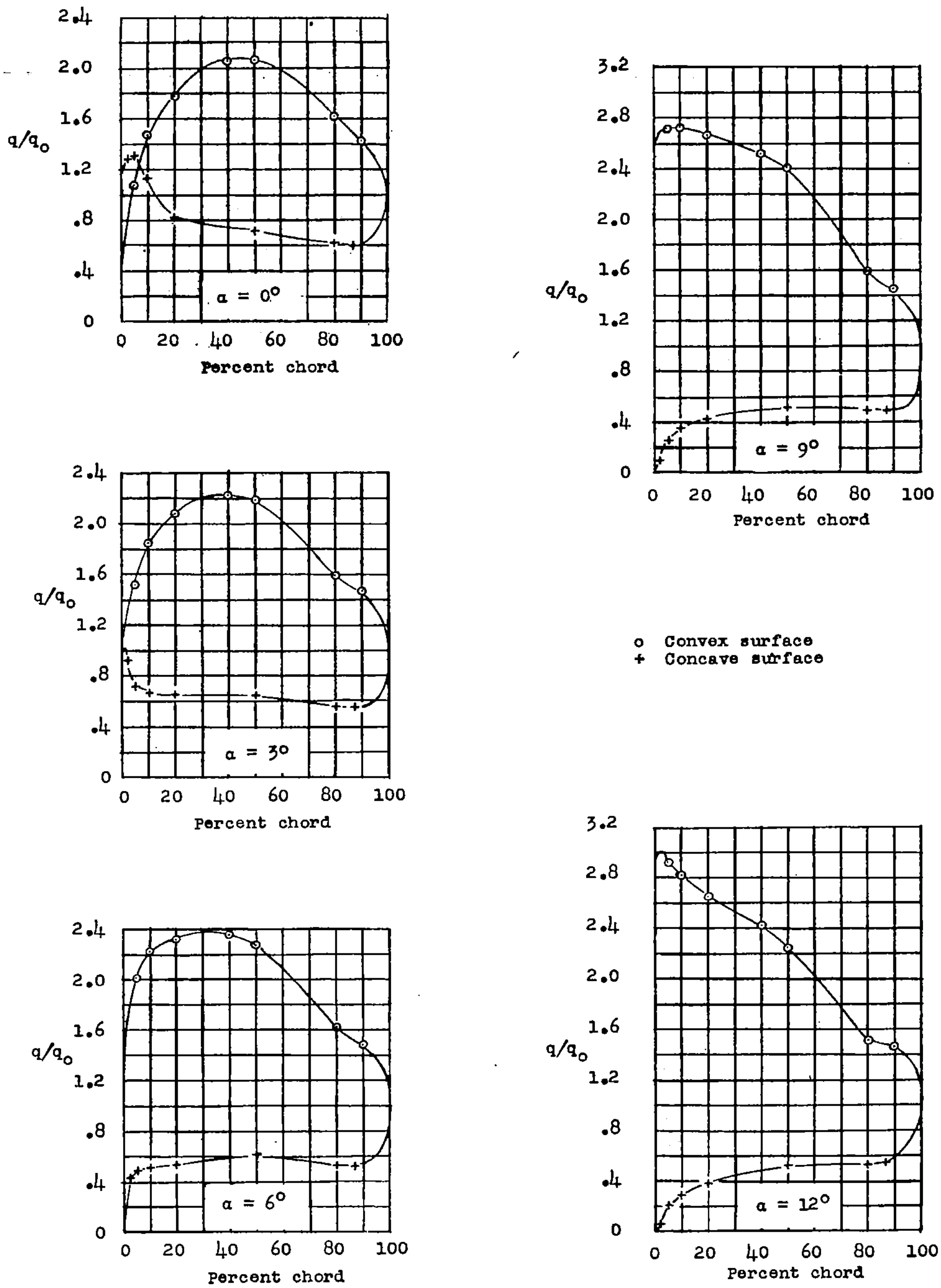

NATIONAL ADVISORY COMMITTEE FOR AERONAUTICS

Figure 34.- Section pressure distributions. Isolated NACA 65-(18)10 blower-blade section; α_d = 5.5°.

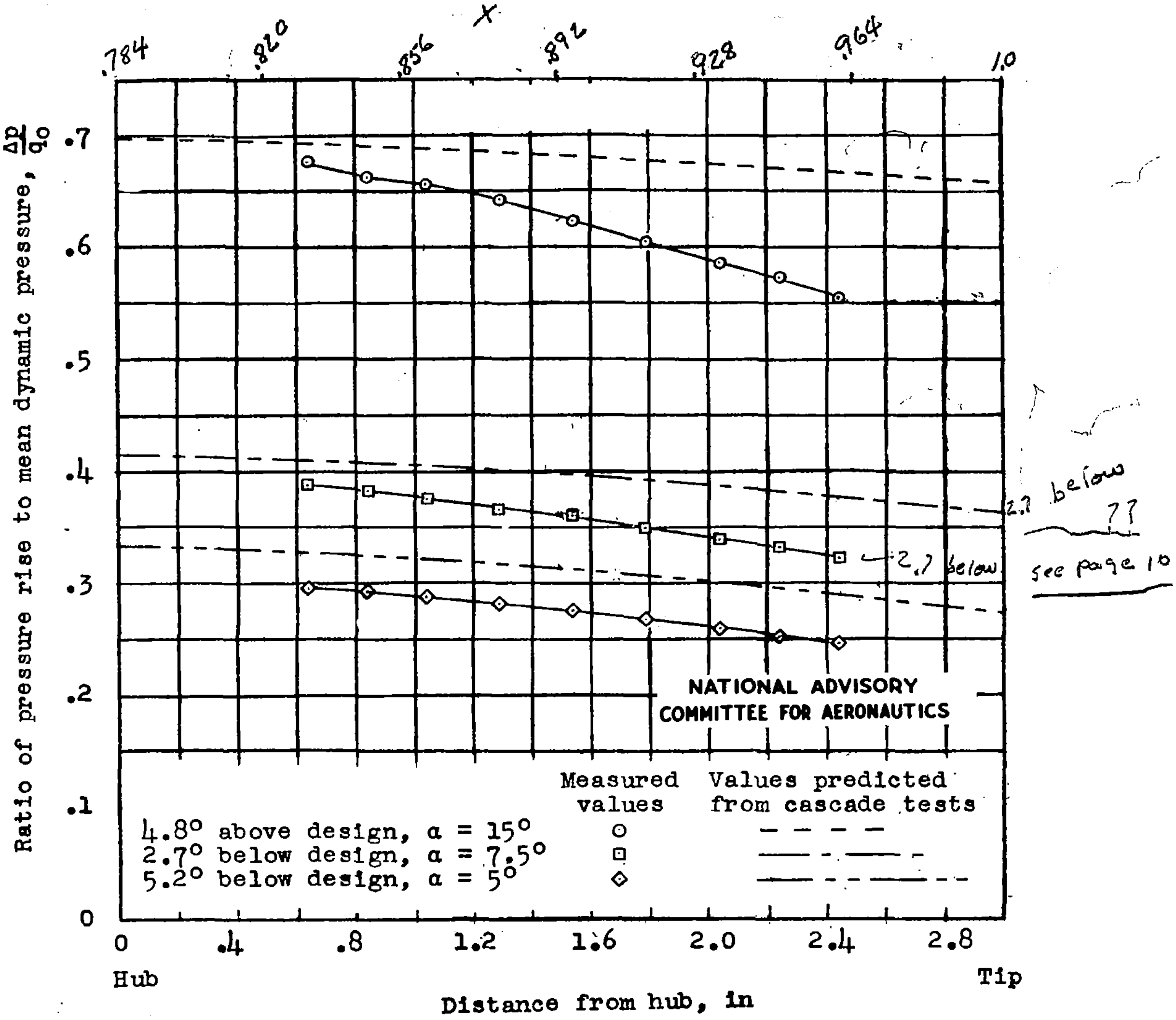

Figure 35.- Variation of ratio of pressure rise to mean dynamic pressure along the blade showing a comparison of measured values from test blower and values predicted from cascade turning angles.

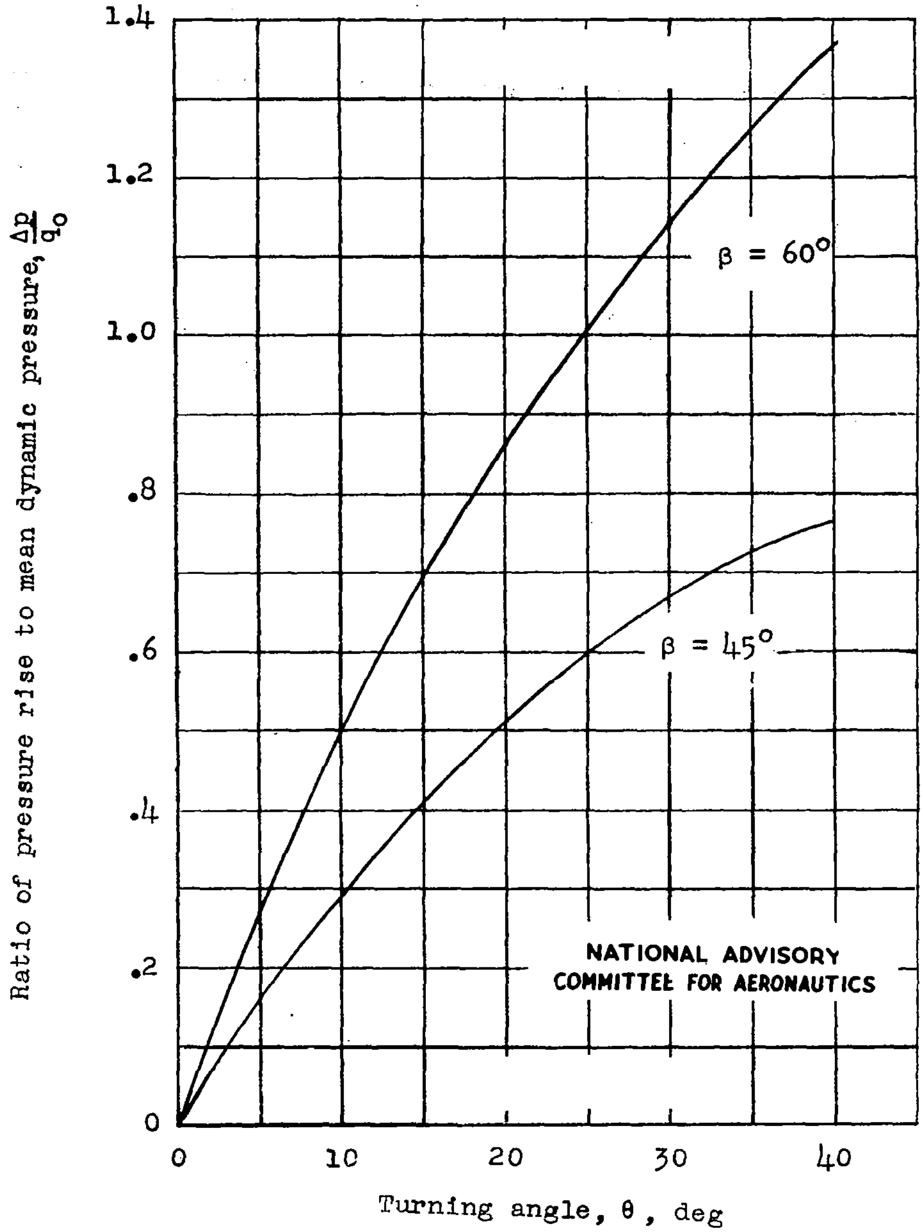

Figure 36.- Variation of theoretical $\Delta p/q_o$ with turning angle for the two conditions of stagger tested.

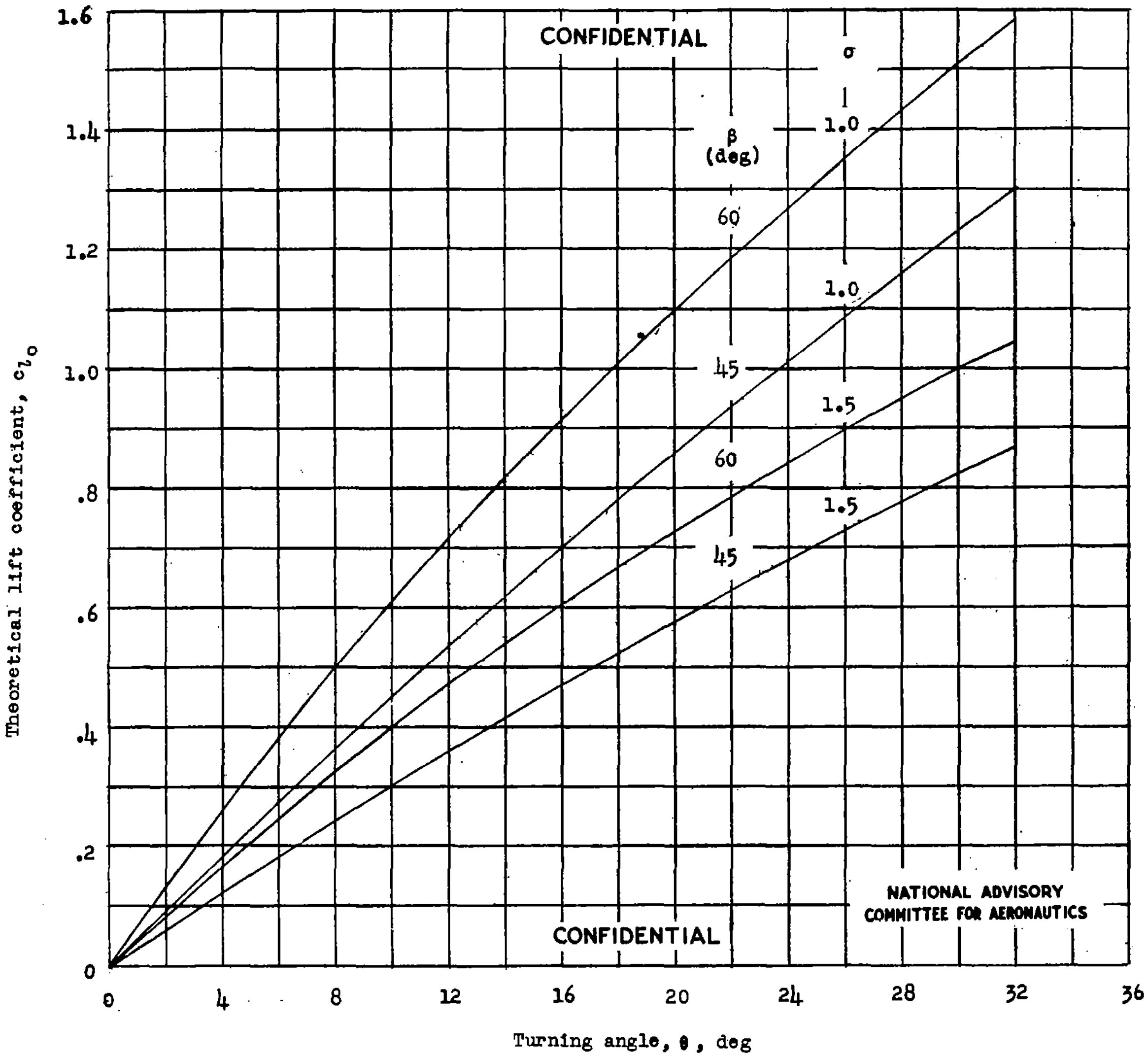

Figure 37.- Variation of theoretical lift coefficient with turning angle for cascade setups tested.

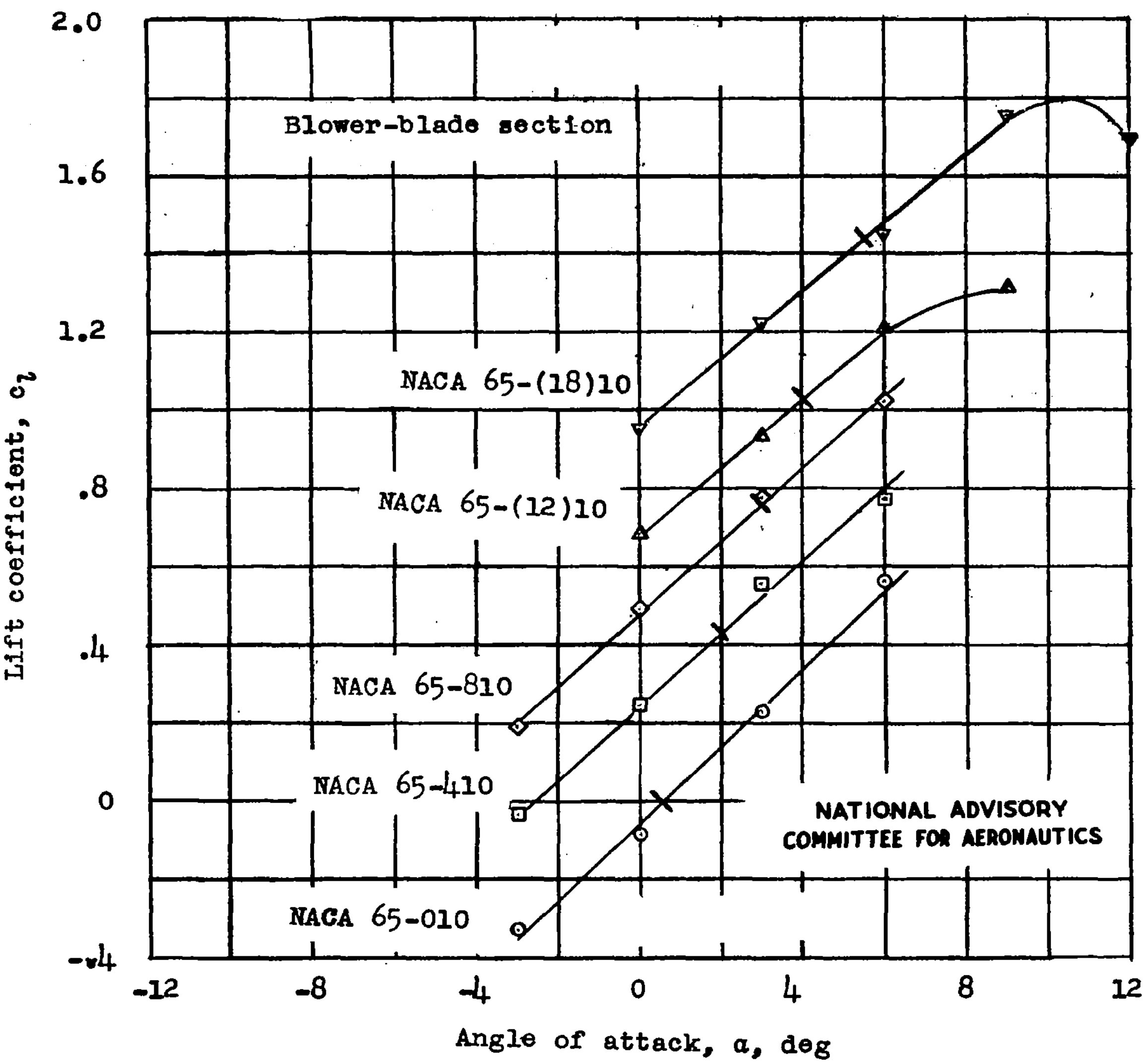

Figure 38.- Lift characteristics of five NACA 65-series blower-blade sections tested as isolated airfoils. (Short line across curve designates design point.)

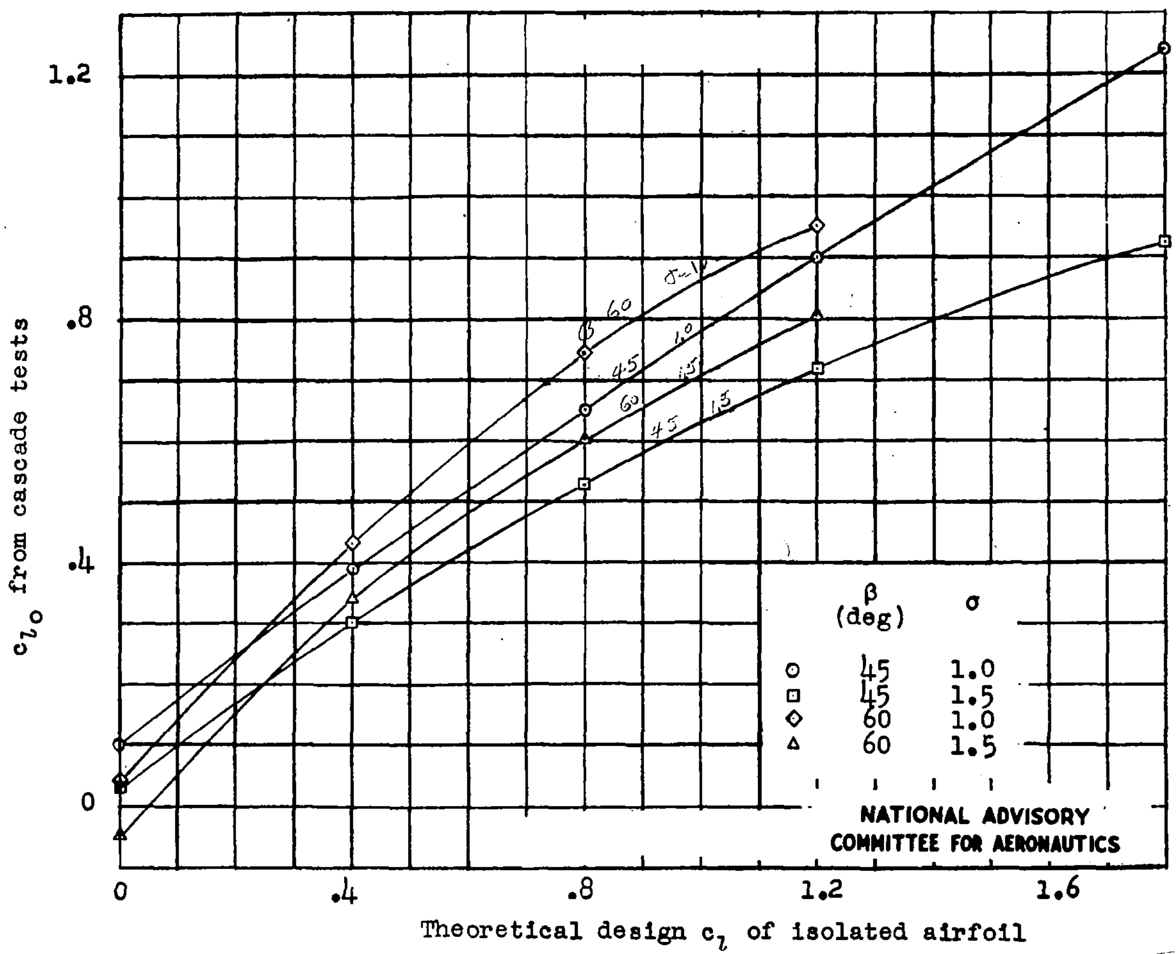

Figure 39.- Comparison of c_l of airfoil in cascade with theoretical design c_l of isolated airfoil.

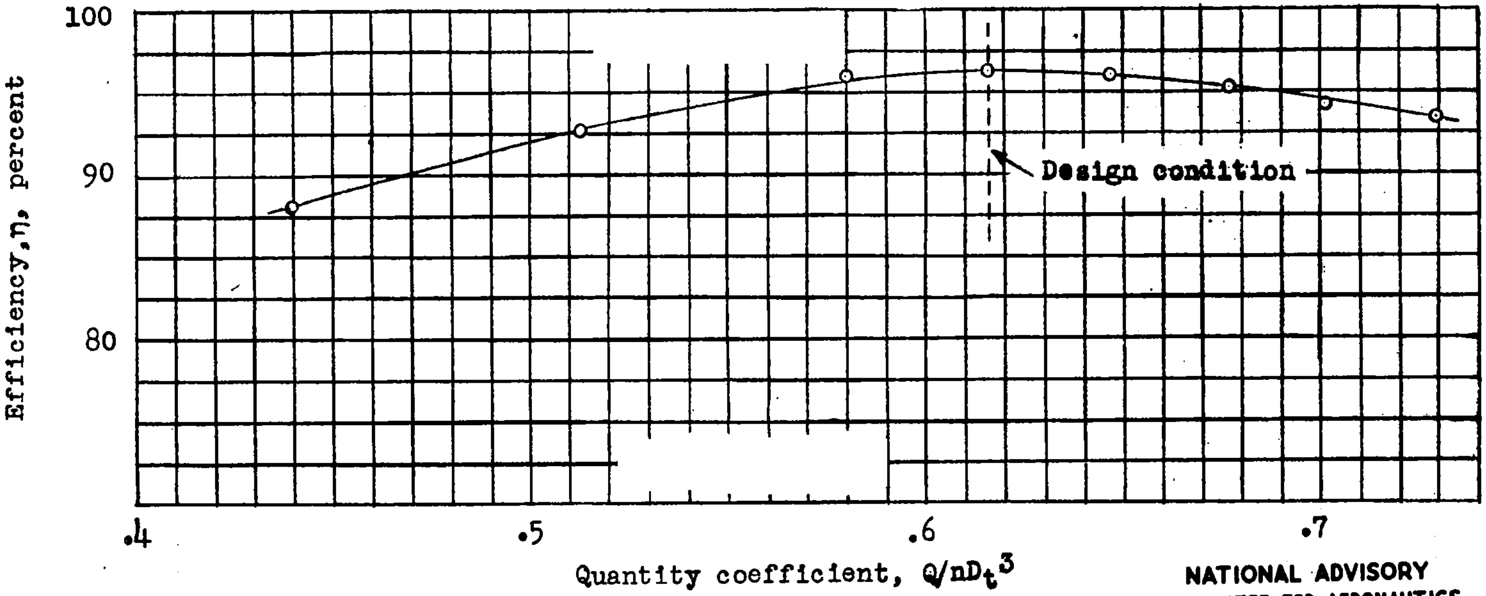

Figure 40.- Efficiency characteristics of test rotor showing predicted design condition.

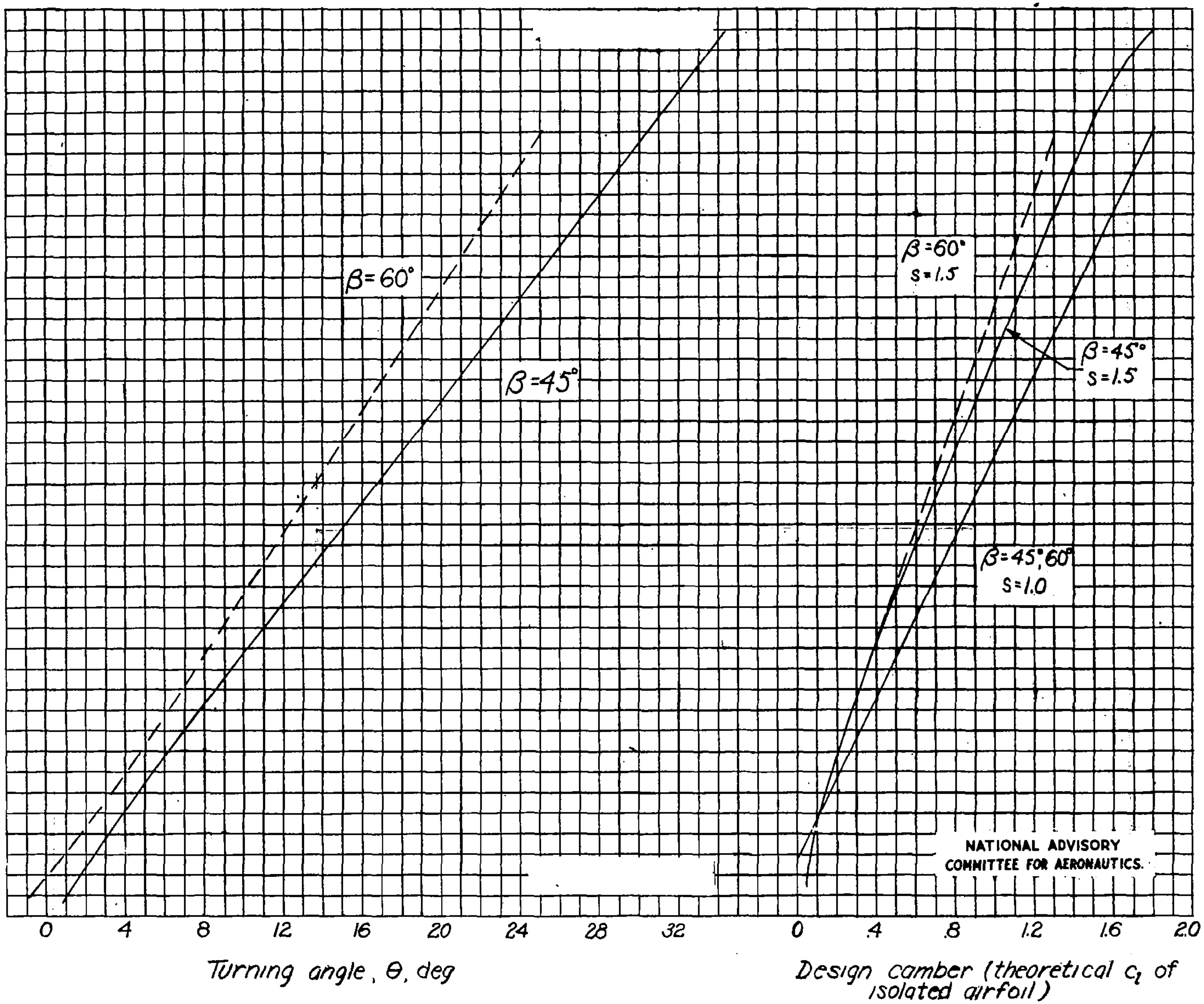

(a) Relation between turning angle and design camber.

Figure 41.-Fan and compressor blade design charts; NACA 65-series blower blades.

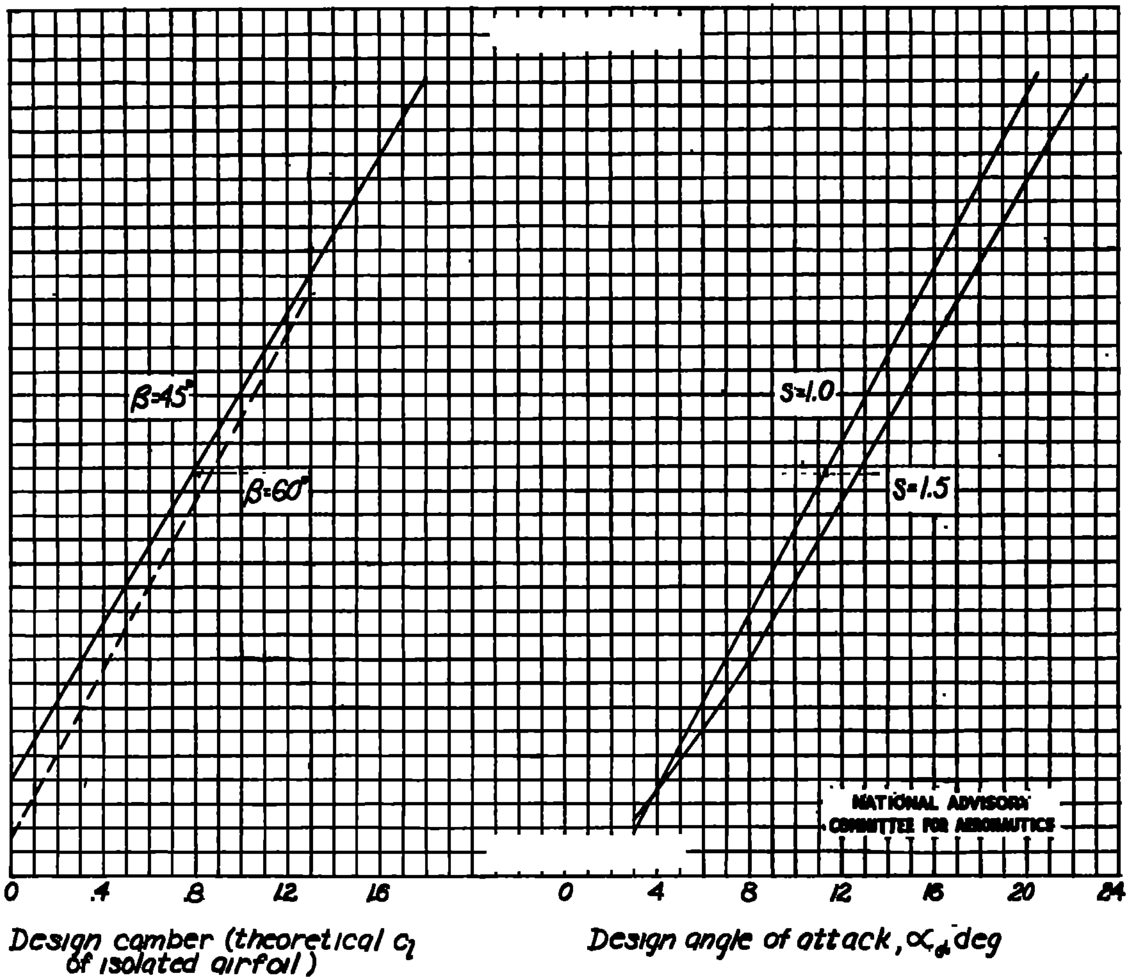

(b) Relation between design camber and design angle of attack.

Figure 41.–Concluded.

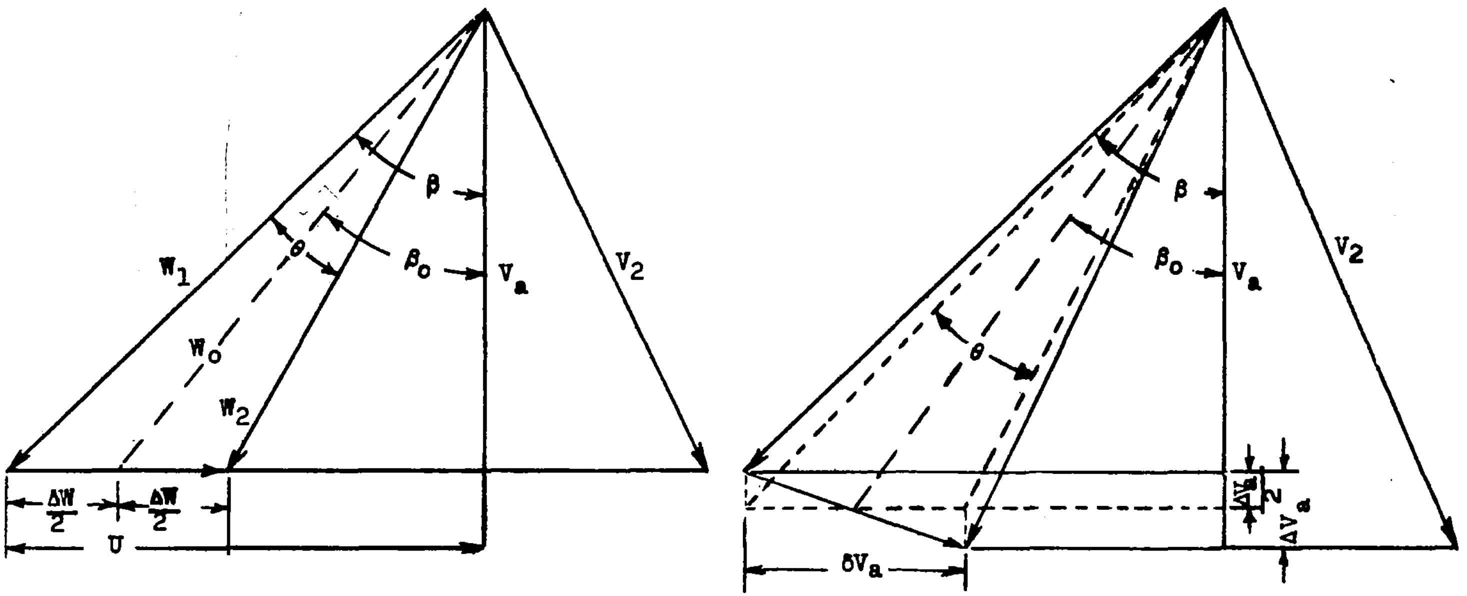

(a) Constant axial velocity.

(b) Varying axial velocity.

Figure 42.- Typical vector diagrams for axial-flow fans and compressors.